Analyst

CRITICAL REVIEW

View Article Online
View Journal | View Issue

Cite this: *Analyst*, 2018, **143**, 3230

Electrochemiluminescence biosensing based on different modes of switching signals

Ying Zhuo, † Hai-Jun Wang,† Yan-Mei Lei, Pu Zhang, Jia-Li Liu, Ya-Qin Chai * and Ruo Yuan *

Received 12th February 2018,
Accepted 18th May 2018

DOI: 10.1039/c8an00276b

rsc.li/analyst

Electrochemiluminescence (ECL) has attracted much attention in various fields of analysis owing to low background signals, high sensitivity, and excellent controllability. In recent years, to further boost the performance of biosensors, diverse output signal modes have been developed, which exhibited respective advantages. In this review, we summarize the latest sensing applications of ECL bioanalysis by generalizing different output signal modes and give future perspectives for new developments in ECL analytical technology.

1. Introduction for ECL technology

Electrochemiluminescence (ECL), also called electrogenerated chemiluminescence, is a kind of chemiluminescence (CL) phenomenon powered by electrochemical means. By the smart integration of electrochemistry and spectroscopy, ECL has shown potential superiorities over other optical methods. First, compared with fluorescence, ECL has no need for external light sources, which not only simplifies the experimental apparatus but also disables background responses from luminous impurities and scattered light, thus resulting in high sensitivity. Second, ECL shows preferable control toward the position of the luminous emission because ECL emission is close to the surface of the electrode. Third, it has an excellent specificity owing to the relationship between the ECL species and co-reactants, and satisfied selectivity since the excited states can be operated by alternating the applied potential. Finally, ECL allows better control over the time of ECL systems, improving their simplicity and reproducibility. Therefore, the ECL technique has become one of the most powerful analytical tools in the field of trace target detection, food and environmental monitoring, imaging, *etc*.

With the fast developing of ECL analysis, researchers realized several modes of switching a signal for ECL biosensing and ECL imaging. This review presents a detailed summary of the biological applications of ECL that are based on different switching modes. In particular, this review has tried to make an in-depth discussion and conclusions on the similarities and differences of ECL biosensing through a single channel and multiple channels.

Key Laboratory of Luminescent and Real-Time Analytical Chemistry (Southwest University), Ministry of Education, College of Chemistry and Chemical Engineering, Southwest University, Chongqing 400715, PR China. E-mail: yuanruo@swu.edu.cn, yqchai@swu.edu.cn; Fax: +86-23-68253172; Tel: +86-23-68252277
† These authors contributed equally to this work.

2. Different signal output modes of ECL biosensors

2.1 Single signal switching modes

Single signal switching modes have been widely employed in either "signal-off" or "signal-on" modes over the past several decades. Correspondingly, the signal either decreases or increases in response to the presence of analytes. In general, the signal-off modes as a powerful approach have been demonstrated to be significantly prospective for a sensing platform due to its high sensitivity, facile manipulation, reagentless process, and so on.[1–3] According to different ways of using the quenching mechanism, we classify the "signal-off" modes into four broad categories.

2.1.2 Signal-off

2.1.2.1 Signal-off induced by ECL quencher. The ECL emission of the luminophore is directly quenched by the ECL quencher, making the ECL signal decreases with the increasing concentrations of analytes.[4] Over the past few years, extensive efforts have been made to establish a traditional "signal-off" mode for target detection.[5] Notably, the quencher is a fundamental and important material for the construction of the signal-off bioanalysis strategy based on electron transfer. For example, ferrocene (Fc) as a classic quencher has been demonstrated by Cao *et al.*[6,7] to quench the ECL emission of $Ru(bpy)_3^{2+}$ *via* electron transfer. Moreover, Quantum dots (QDs) have been widely utilized in ECL sensors due to their beneficial physical properties such as broad excitation and symmetric tunable emission spectra, photochemical stability, and binding compatibility with biomolecules. Therefore, Ju's group

proposed that a ferrocenyl-terminated dendrimer as quencher be constructed to quench the cathodic ECL emission of QDs; this made the ECL intensity drop notably due to the enrichment of Fc molecules.[1] Lately, the construction of a novel and highly-effective quenching method has become a particular focus in practical applications of biosensor assays for accomplishing highly sensitive detection. As shown in Fig. 1, Chen *et al.* developed a "signal-off" ECL platform for thrombin by controlling the distance between CdS nanocrystals (NCs) and Au nanoparticles (NPs) and the enhanced ECL of CdS NCs with Au NPs based on energy transfer.[8] They synthesized CdS NCs as an ECL emitter and attached an aptamer of thrombin. The single-stranded DNA–Au nanoparticle (ssDNA–AuNP) conjugates were formed after modification of complementary ssDNA on a CdS NCs modified electrode. An enhanced ECL signal was achieved because of energy transfer between AuNPs and CdS NCs with a separation length. Significantly, such ECL signal enhancement may be the most import and novel point in the "on–off" switch system construction for improving detection sensitivity as compared to the traditional "signal-off" modes. The ECL signal decrease was achieved by target-induced removal of ssDNA–AuNP conjugates, greatly reflecting the presence of target protein. Moreover, decrease of the ECL signal was logarithmically linear with the concentration of thrombin in a wide range from 100 aM to 100 fM. Summarized from the above examples, the single quenching path was usually designed in a signal-off biosensor construction. Thus, it can be concluded that the key point is that the more highly the initial signal of the "signal-on" state was enhanced, the larger the quenching rate of the "signal-off" state became, as well as the lower the background signal was.

Moreover, with a high initial ECL signal as the desirable "signal-on" state and a multi-quenching as an excellent "signal-off state", an elaborated system provided a new chance for constructing a variety of the highly sensitive "signal-off" modes. Thus, in our previous work, a novel "on–off" ECL aptasensor was developed based on multi quenching of the hemin/G-quadruplex DNAzymes towards the Ru(II) self-enhanced molecule (PTCA-PEI-Ru(II))-based ECL system for highly sensitive determination of thrombin (Fig. 2).[9] First, based on the dual amplification strategies which are outlined as follows: (i) an intermolecular co-reaction between PTCA-PEI-Ru(II) and nicotinamide adenine dinucleotide (NADH) and (ii) an intramolecular self-enhanced PTCA-PEI-Ru(II), a strong initial ECL signal was achieved as the signal-on state. Then, the signal-off state was realized by the strategy of (i) consuming the co-reactant of NADH which originated from the hemin/G-quadruplex DNAzymes to oxidize NADH and *in situ* generate the H_2O_2; (ii) the active center of hemin could oxidize the excited state Ru(II) * to Ru(III), making the energy and electron transfer quench; and (iii) hemin/G-quadruplex DNAzymes could act as horseradish peroxidase (HRP) to catalyze H2O2 for *in situ* producing the quencher of O_2. Down to the femtomolar level of thrombin was detected by the novel triple quenching effect of multifunctional hemin/G-quadruplex DNAzymes upon the Ru(II) self-enhanced complex-based ECL system. With the design of the "on–off" switch, the proposed aptasensor was anticipated to apply in determination of other targets.

2.1.2.2 Signal-off induced by ECL-RET. An efficient sensing platform based on electrochemiluminescence resonance energy transfer (ECL-RET) was developed to further boost the sensitivity of ECL sensors. ECL-RET, often occurring between an effective energy donor and a suitable acceptor, is an attractive technique for sensitive detection of analytes due to its no excitation light source and no interference from the scattered light.[10–12] Chen's group developed a sensitive biosensor based on a ECL-RET protocol with Au@Ag_2S NPs as the ECL acceptor and $Ru(bpy)_3^{2+}$ composites (graphene oxide(GO)-Au/RuSi@$Ru(bpy)_3^{2+}$/chitosan(CS)) as the ECL donor.[13] Significant advantages were acquired for ultrasensitive detection of nucleotide sequences, proteins and cells. Especially, the critical step to

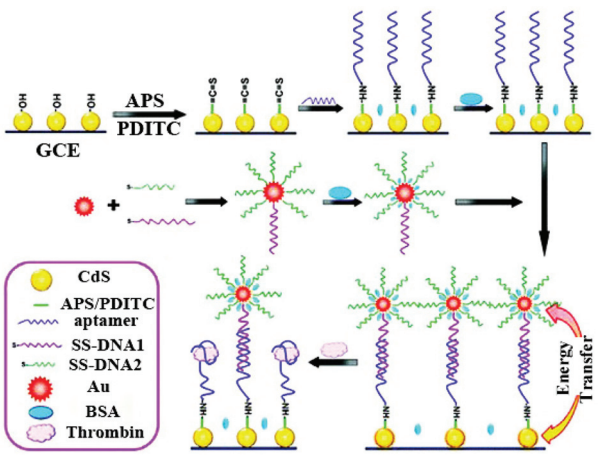

Fig. 1 Illustration of the ECL enhancement of CdS NCs by Au NPs and "signal-off" ECL strategy originating from the replacement of ssDNA–AuNP conjugates by a target. (Reprinted with permission from ref. 8. Copyright 2011 American Chemical Society.)

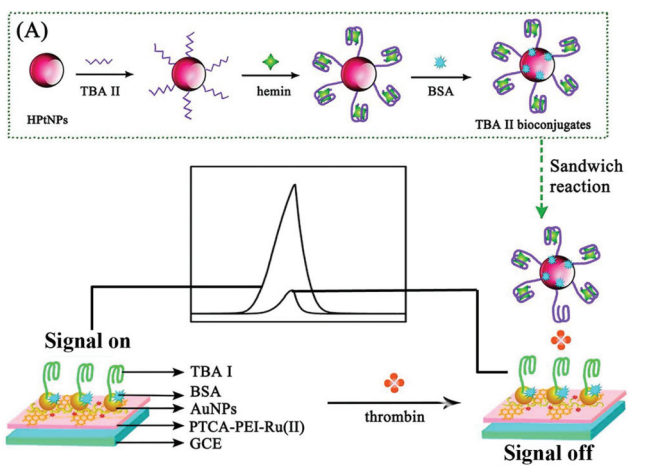

Fig. 2 Schematic illustration of the possible luminescence mechanism of the "on–off" ECL aptasensor. (Reprinted with permission from ref. 9. Copyright 2015 American Chemical Society.)

Table 1 The ECL-RET systems fabricated using different kinds of donors and acceptor

Donor	Acceptor	Ref.
CdS QDs	$Ru(bpy)_3^{2+}$	19
g-C_3N_4 NS	$Ru(bpy)_3^{2+}$	20
CdS NRs	$Ru(bpy)_3^{2+}$	21
CdS QDs	Cy5	22
$Ru(dcbpy)_3^{2+}$	CdSe@ZnS QDs	23
CdS QDs	Ag CNs	24
CdS QDs	Au NPs	25
$Ru(bpy)_3^{2+}$	CdTe QDs	26
CdTe QDs	TAEA-Ru	27
CdS:Eu QDs	Au NRs	28
CdS:Eu QDs	Au NPs	29
BSA-AuNC	$Ru(bpy)_3^{2+}$	30
G QDs	Au NPs	31
PTC-NH_2	$S_2O_8^{2-}$	14
$([Ru(bpy)_3]^{2+})$/2-(dibutylamino) ethanol	CdSe@ZnS QDs	32
$Ru(bpy)_3^{2+}$	AuNPs/GO	33
GO-Au/RuSi@$Ru(bpy)_3^{2+}$/CS	Au@Ag_2S	34
Pb(II)-β-cyclodextrin	CS/$Ru(bpy)_3^{2+}$/silica NPs	35
CdTe/CdS QDs	AuNRs	36
Si QDs	Au NPs	37
NGQDs	Fe_3O_4@MnO_2	38
Luminol	$Ru(bpy)_3^{2+}$	39
Luminol	CdSe@ZnS QDs	40
Si-Containing polymer dots	DA	41

obtain optimal ECL-RET efficiency is to search for the perfect energy overlapped donor–acceptor pair (Table 1).

Herein, our group constructed a ratiometric sensing platform for lead ion detection based on ECL-RET between peroxydisulfate/oxygen as a donor and the perylene derivative as an acceptor.[14] Apparently, it is significant to look for a new donor–acceptor pair because energy-tunable materials show great application potential to realize an ECL-RET for enhancing the ECL intensity. Therefore, various kinds of nanocomposites such as Au NPs/GO,[15] CdS/graphene,[16] and hemin/graphene/gold nanorods (H/RGO/Au NRs)[17] were also used as acceptors.

For example, Zhu's group reported a convenient and simple biosensing approach based on ECL-RET between luminol as a donor and CdSe@ZnS quantum dots (CdSe@ZnS QDs) as an acceptor in neutral conditions (Fig. 3).[12] The thrombin binding aptamer (TBA) covalently functionalized the CdSe@ZnS QDs/GCE *via* an amidation reaction between the carboxyl group on the CdSe@ZnS QDs surface and the amino group of TBA. After hybridizing with TBA, the DNA probe was successfully immobilized on the modified electrode. Another layer of CdSe@ZnS QDs was connected to the DNA probe, and an enhancement of anodic ECL intensity was achieved due to the ECL-RET between the CdSe@ZnS QDs and the excited state of luminol. Once thrombin displaced the probe DNA due to its higher affinity for TBA, then sensitive detection of thrombin can be achieved. Upon ECL-RET, the as-proposed luminol-CdSe@ZnS QDs ECL biosensor yielded a linear range from 10 fM–100 pM, which will be a promising way for the analysis of protein. Summarizing from the above examples, "signal-off" strategies induced by ECL-RET strategies are springing up and

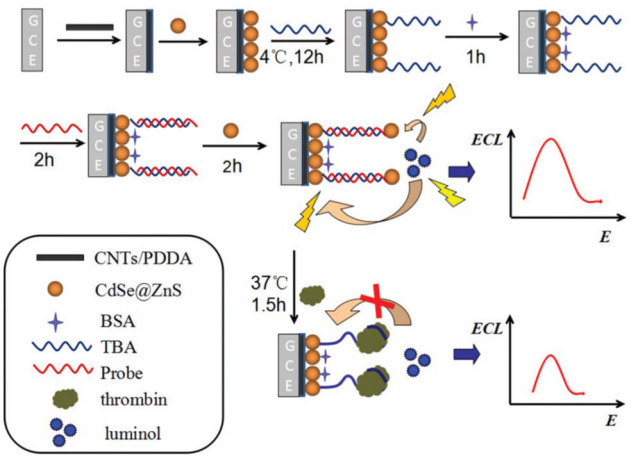

Fig. 3 Schematic representation of the modification of GCE and detection of thrombin. (Reprinted with permission from ref. 12. Copyright 2014 American Chemical Society.)

have now become the main driving force of innovation for ECL assays.

The above study demonstrated an intermolecular ECL-RET between CdSe@ZnS QDs and luminol, which was an efficiency strategy for biological applications. Although the method has improved the sensitivity of the sensors to a certain extent, the ECL-RET still suffers from a defect of low energy transfer efficiency. More recently, as shown in Fig. 4, our group employed the intramolecular ECL-RET between luminol as donor and $Ru(bpy)_3^{2+}$ as an acceptor due to a perfect spectral overlap of the donor and acceptor.[18] In brief, a high ECL signal was obtained through the intramolecular ECL-RET from the luminol excited state to $Ru(bpy)_2(mcpbpy)^{2+}$ in the Lum-Ru. Then, after the sample solution (containing dNTPs, Nt. BbvC I nicking enzyme, phi29 polymerase, and the target afla-

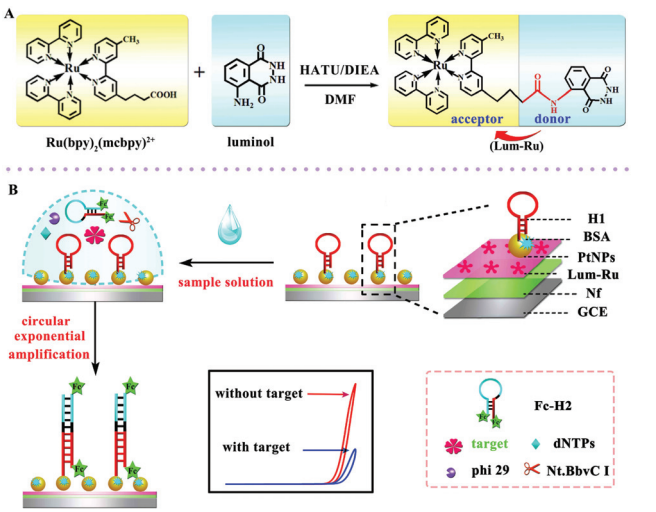

Fig. 4 Representations of (A) the synthesis of the Lum-Ru compounds and (B) fabrication of the aptasensor and the reaction mechanism. (Reprinted with permission from ref. 18. Copyright 2017 Wiley.)

toxin M1 (AFM1)) was incubated on the modified electrode and a one-pot target-induced circular exponential amplification (TICEA) was executed to recycle AFM1 and produced numerous ssDNA as the "mimic target". Eventually, a mass of hairpin probe 1 (H1) on the surface of the electrode was opened to form numerous ferrocene-labeled double stranded DNA (dsDNA) resulting in a significant decrease of ECL intensity from the ferrocene quenching. Thus, the proposed aptasensor achieved quantitative detection of AFM1 through the change of ECL response to the concentration of AFM1 with high sensitivity. In general, with a highly-efficient ECL-RET in one molecule, a highly intense ECL signal of Lum-Ru was obtained owing to the short path of energy transmission and less energy loss between luminol and $Ru(bpy)_2(mcpbpy)^{2+}$.

2.1.2.3 Signal-off induced by steric hindrance. Steric hindrance from a target induced deposition or biorecognition reaction was usually designed in a signal-off biosensor construction.[42] Steric hindrance could suppress the ECL signal from the electrode surface, which has enabled the development of signal-off ECL sensing systems.[43,44] From the decrease of an ECL signal caused by physical effects, researchers have greatly improved performance by bringing in nanomaterials to improve ECL intensity and offering more binding sites, which is suitable for the sensing of biomacromolecules and cells.[45,46] As shown in Fig. 5, using a steric hindrance effect, Jiang's group constructed a one-step ECL immunosensor for sensitive detection of carbohydrate antigen 19-9 (CA19-9).[47] In this system, a magnetic graphene oxide nanomaterial ($nanoFe_3O_4$@GO) was synthesized for CA19-9 antibody (anti-CA19-9) binding and *N*-(4-aminobutyl)-*N*-ethylisoluminol (ABEI) loading. The multi-functionalized magnetic nanomaterial then was immobilized on the GCE surface in the presence of an external magnetic field. Finally, the ECL immunosensor was established based on a one-step direct immunoreaction process for ultrasensitive detection of CA19-9 with a detection limit of 0.0005 U mL^{-1}.

In a novel solid-state ECL sensor based on a steric hindrance effect reported by Fu's group (Fig. 6),[48] a ECL "on–off" sensor with a luminescence-functionalized ruthenium metal–organic framework (Ru-MOF) nanoflowers and CdS QDs was

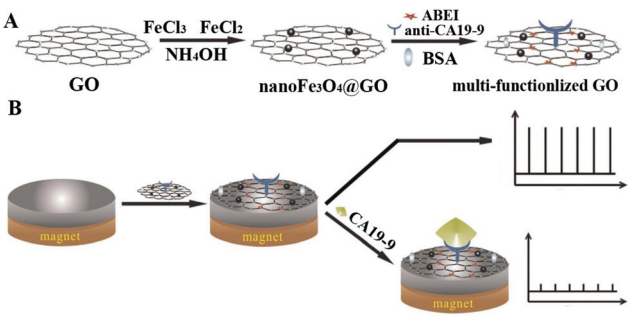

Fig. 5 Schematic diagram for (A) the preparation of multi-functionalized graphene oxide, and (B) the fabrication and application protocol of the ECL immunosensor using multi-functionalized graphene oxide. (Reprinted with permission from ref. 47. Copyright 2015 Elsevier.)

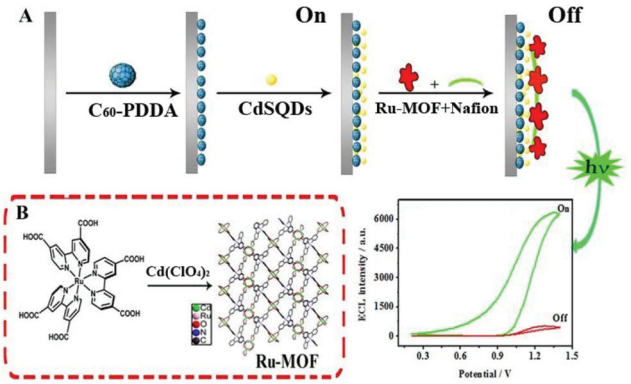

Fig. 6 (A) Schematic illustration of the ECL sensor. (B) Preparation of the Ru-MOF. (Reprinted with permission from ref. 48. Copyright 2017 Elsevier.)

developed as a "signal-off" switching sensor. The presence of tryptophan significantly inhibited the ECL signal from the electrode surface to achieve efficient reduction of the signal for tryptophan enantiomers detection. This "on–off" strategy may open new channels based on novel switches for sensing small molecules. And we expect that it will promote the development of nanomaterials-based sensors and improve their performance in a range of important applications. As depicted in Fig. 7, a non-labeled ECL immunosensor with the use of CdSe QDs for detection of human prealbumin (PAB) has been described based on a similar inhibition process.[49] Specifically, cysteamine was first modified on the gold electrode surface and then conjugated with the Au NPs cysteine, anti-PAB (PAB antibody), and CdSe QDs *via* an amide bond. In the presence

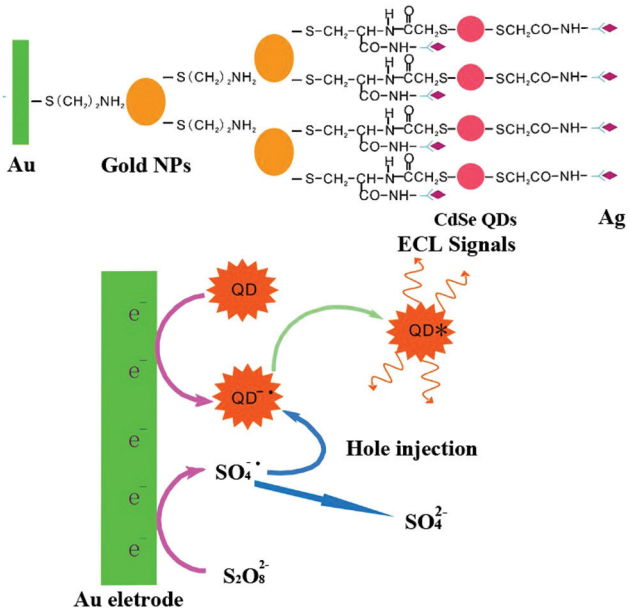

Fig. 7 Schematic illustration of fabrication process (A) and ECL mechanisms (B) of the ECL immunosensor. (Reprinted with permission from ref. 49. Copyright 2008 Elsevier.)

of PAB, the immunocomplex generated and inhibited the reaction between $K_2S_2O_8$ with CdSe QD since the increase of the steric hindrance, eventually resulting in a decrease of ECL intensity. Although this system is simple and convenient, its sensitivity is limited, and it is difficult to realize the sensitive analysis of a constant target.

2.1.2.4 Signal-off induced by nucleic acid-based cutting strategy. Recently, signal-off strategy based on DNA enzyme (DNAzyme) has become an interesting alternative for sensitive detection of targets. Among various strategies, endonucleases and exonucleases were mainly utilized, and sensors were based on which were developed.[50,51] Accordingly, many works have been done on utilizing endonucleases such as restriction endonucleases Nt.AlwI,[51] EcoRI,[52] T7 exonuclease (T7Exo),[53] and so on. For example, as displayed in Fig. 8, our group had constructed a restriction endonucleases (Nt.AlwI)-powered DNA walking machine for sensitive detection of target DNA.[54] With the help of Nt.AlwI, the walker (the target DNA) was induced in an autonomous and directional stepwise movement of the walker along the DNA track which was driven by the cleavage of the Ru(bpy)$_2$phen-containing stators, leading to significantly decreased ECL signals for a highly sensitive detection of the walker. In addition, using DNA as the architectural scaffolds, a DNA walker can have great potential for building up a sensitive and specific biosensor.

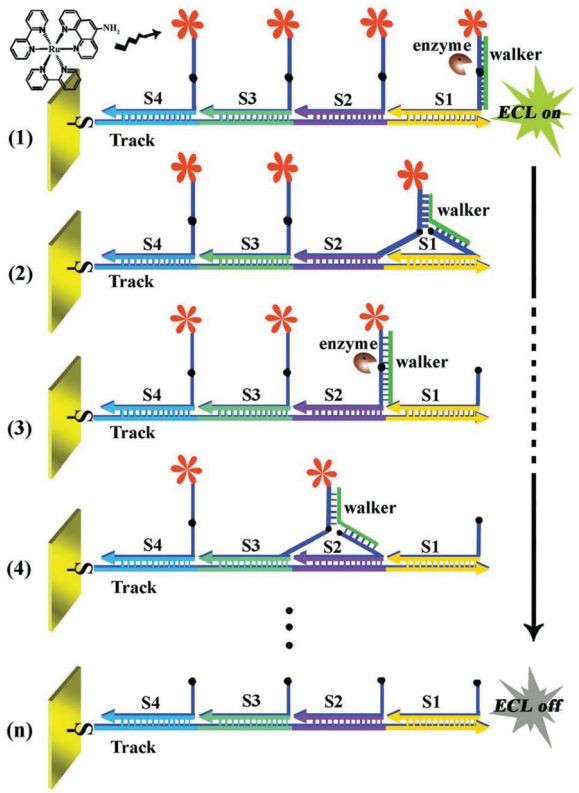

Fig. 8 Working principle of the restriction endonucleases-powered DNA walking machine. (Reprinted with permission from ref. 54. Copyright 2015 Royal Society Chemistry.)

Through the endonuclease-stimulated regeneration of the analyte, the aptasensor which focused on improving the sensitivity of target detection is highly desired. Alternatively, on the basis of site-specific cleavage of BamHI endonuclease and enzymatic signal amplification, an electrochemical method to detect the hepatitis C virus was developed. In this case, as show in Fig. 9, Dai's group had designed a novel strategy based on site-specific cleavage of BamHI endonuclease combined with bidentate chelation of the dithiocarbamate DNA (DTC-DNA) probe and the ECL activity of GQDs assembly.[55] Using hepatitis C virus-1b genotype complementary DNA (HCV-1b cDNA) as a model, the BamHI endonuclease site-specifically recognized and cleaved the duplex symmetrical sequence 5′-GGATCC-3′, which made the dsDNA fragments and graphene quantum dots (GQDs) break off from the electrode surface, leading to a decline of the ECL intensity.

On the basis of variations of the ECL intensity before and after digestion of the DNA hybrid, a novel "signal-off" ECL system was developed. With reliance on the instinctive properties proposed above, we anticipate that this sensing strategy can be expanded to explore an extensive range of DNA targets with reasonable design and hold significant potential bioanalysis.

Moreover, due to the high catalysis efficiency and substrate specificity of nucleases, nuclease-based target cycling has been widely used in the field of highly sensitive biological analysis. For example, as depicted in Fig. 10, Chen's group[56] reported an ultrasensitive and selective ECL biosensor with the use of G-quadruplex-based DNAzyme as the electrocatalyst for the reduction of H_2O_2, based on K-doped graphene/CdS:Eu QDs and nicking endonuclease assisted strand-scission cycle, which resulted in an obvious decrease in ECL intensity and thus achieved sensitive DNA detection. Besides, exonuclease cleavage of DNA also plays an important role in medicinal chemistry and biological fields. In addition, enzymatic DNA

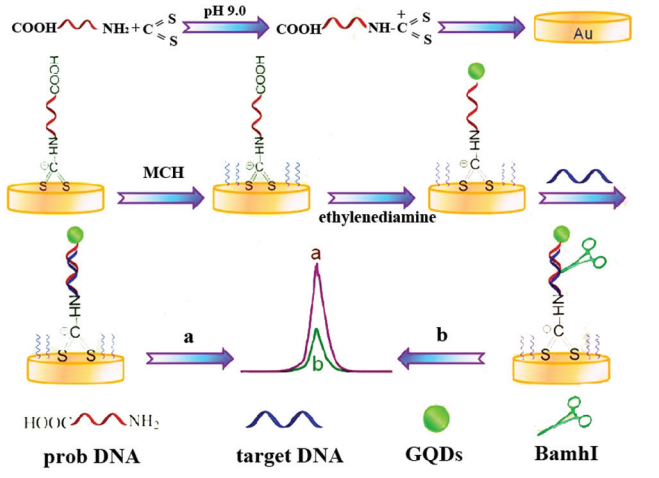

Fig. 9 Schematic illustration of the ECL biosensor based on GQDs combined with endonuclease cleavage and bidentate chelation. (Reprinted with permission from ref. 55. Copyright 2015 American Chemical Society.)

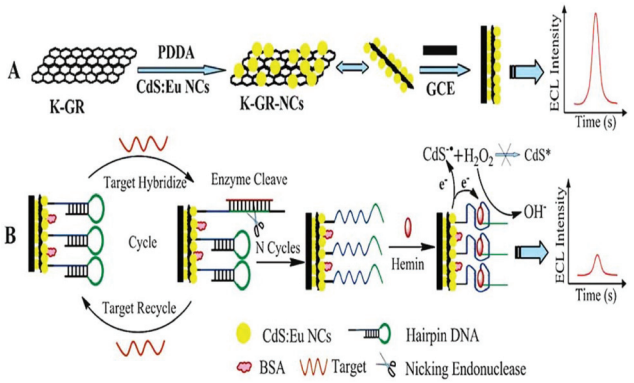

Fig. 10 Schematic representation of the proposed ECL-DNA biosensor. (Reprinted with permission from ref. 56. Copyright 2013 Royal Society Chemistry.)

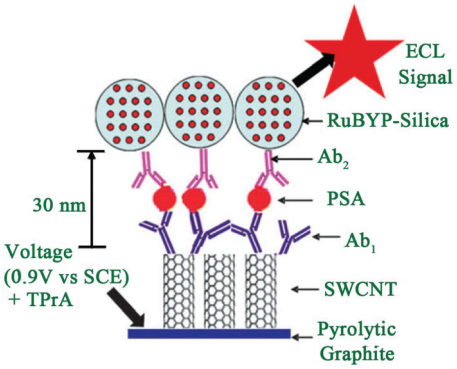

Fig. 11 Scheme of representation of ECL-based SWCNT immunosensors after addition of PSA and $[Ru\text{-}(bpy)_3]^{2+}$-silica-Ab_2 nanoparticles. (Reprinted with permission from ref. 63. Copyright 2009 Royal Chemical Society.)

circuits could achieve high sensitive analysis which have been proposed and drawn particular interest in biosensing.

2.1.3 Signal-on. Signal-on, an inverse signal output mode of biosensor compared with signal-off mode, is processing of a signal from weak to strong before and after the target recognition. It is a popular ECL signal output mode with wide detection range and low background signal in principle and has emerged as an efficient method for immunoassay, nucleic acid analysis and metallic ion detection.[57–59] The methods to realize signal-on are divided into four types: (i) introduction of luminophores; (ii) regulation of the ECL co-reaction; (iii) ECL-RET, and (iv) nucleic acid based amplified strategy.

2.1.3.1 Signal-on induced by introduction of luminophores. Usually, to construct a signal-on mode in an ECL biosensor, luminophores are introduced into the sensing interface through a sandwich immunoassay or sandwich-like immunoassay based on the target identification. A Ru complex,[60] luminol and its derivatives,[61] quantum dots,[62] and, as usual ECL regents have been applied in many fields especially ECL immunosensors, nucleic acids biosensors, and aptamer sensors. Usually, a sandwich immunoassay format is the typical method in a signal-on-type ECL biosensor. Briefly, the primary antibody(Ab_1) is immobilized on an electrode to capture the target antigen, then the detection antibody(Ab_2)-bioconjugates, which are labelled by luminophores, can be introduced into the sensing interface after which an obvious ECL signal is obtained. For example, Sardesai and co-workers reported a sandwich immunoassay for prostate specific antigen (PSA) detection (Fig. 11).[63] First, the $[Ru\text{-}(bpy)_3]^{2+}$ doped mesoporous silica nanoparticles were synthesized to prepare Ab_2 bioconjugates ($[Ru\text{-}(bpy)_3]^{2+}$-silica-Ab_2). What's more, single-wall carbon nanotubes were used to chemically attach Ab_1 through an amide reaction. In the presence of PSA, the $[Ru\text{-}(bpy)_3]^{2+}$-silica-Ab_2 bioconjugates could be introduced into the sensing interface to produce a strong ECL signal of $[Ru\text{-}(bpy)_3]^{2+}$. This immunosensor achieved a detection range from 0.04 to 5 ng mL^{-1} with a detection limit of 40 pg mL^{-1}.

With the development of DNA biotechnology, intercalating $Ru(phen)_3^{2+}$ (phen = phenanthroline) in a double stranded (ds)-DNA has emerged as an efficient method for ECL signal-on detection. Yin's group constructed a fragment of five thymidine bases (T_5) immobilized on an electrode to capture the functional oligonucleotide (FO) which had been protected by five adenines at the tail end of $Ru(phen)_3^{2+}$ and intercalating it into double stranded DNA (Fig. 12) which acted as a signal probe.[64] When Hg^{2+} was added, the strong stability and specificity of T-Hg^{2+}-T made FO combine with T_5 to immobilize on the electrode successfully, achieving the increased ECL signal. This biosensor showed high selectivity, as well as a very low detection limit (20 pM). Since the initial ECL signal was

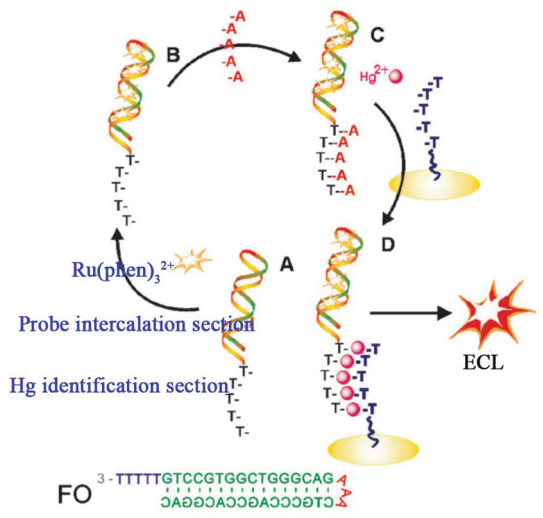

Fig. 12 Schematic illustration of the ECL biosensor for detecting Hg^{2+}. (A) The functional oligonucleotide (FO) containing Hg^{2+} identification and probe intercalation sections; (B) the intercalation of $Ru(phen)_3^{2+}$ into FO; (C) the preformed A-T duplex; and (D) formation of T-Hg^{2+}-T, which results in the introduction of the $Ru(phen)_3^{2+}$ probe onto the electrode surface for ECL determination of Hg^{2+}. (Reprinted with permission from ref. 64. Copyright 2010 Royal Chemical Society.)

relatively low, the ECL biosensor with signal-on mode could achieved high sensitivity.

Luminol, as another important ECL luminophore, was added into detection solutions directly in early ECL assays, and it showed good stability and simple operation,[65] but the relatively high noise was adverse to improving sensitivity. Recently, Cui's group reduced chloroauric acid by luminol directly to produce luminol-capped gold nanoparticles *via* physical adsorptions, which provided an easy and reliable approach for preparing a luminol doped signal tag.[66] Subsequently, the sandwich ECL immunosensor was born at the right time based on this luminol doped signal tag. Li and co-workers achieved label-free ECL immunosensor for cardiac troponin I detection using luminol functionalized gold nanoparticles as a sensing platform with a detection limit of 0.1 ng mL^{-1} (Fig. 13).[67]

2.1.3.2 Signal-on regulated by ECL co-reaction. As is well known, due to the weak signal of an individual ECL luminophore, a co-reactant, for example H_2O_2, TPrA, or $C_2O_4^{2-}$, was usually introduced to obtain an increased ECL signal.[68–74] Therefore, a new signal-on mode was developed based on the regulation from aECL co-reaction. Regulation methods are divided into two kinds: (i) *in situ* generation of a co-reactant, and (ii) introduction of a co-reaction accelerator. Wang and co-workers proposed a versatile ECL immunosensor based on ceria doped ZnO nanoflowers (Ce:ZONFs) for the detection of amyloid-β protein (Aβ). The luminophore of luminol was immobilized on Ce:ZONFs and H_2O_2 was generated *in situ via* a catalytic reaction between glucose and glucose oxidase (GOD) and further catalyzed by Ce:ZONFs to produce ROSs, which promoted the emission of luminol (Fig. 14).[75] This proposed ECL immunosensor had exhibited high sensitivity for Aβ detection with a wide linear range from 80 fg mL^{-1} to 100 ng mL^{-1} and an ultralow detection limit of 52 fg mL^{-1} (Table 2).

To further improve ECL intensity, a co-reaction accelerator has been proposed by our group, which can interact with a co-reactant rather than a luminophore to improve the ECL reaction rate of luminophore and co-reactant. We used semicarbazide as co-reaction accelerator with CdTe QDs-$S_2O_8^{2-}$ to construct an ECL signal-on-type aptasensor for highly sensitive thrombin (TB) detection with a detection limit of 0.03 fM that

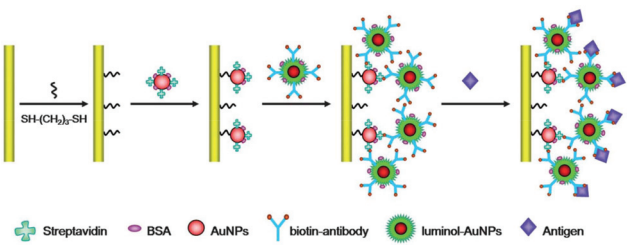

Fig. 13 Schematic illustration of the fabrication processes of the label-free ECL immunosensor using luminol-AuNPs as antibody carriers and sensing platform. (Reprinted with permission from ref. 67. Copyright 2013 Royal Chemical Society.)

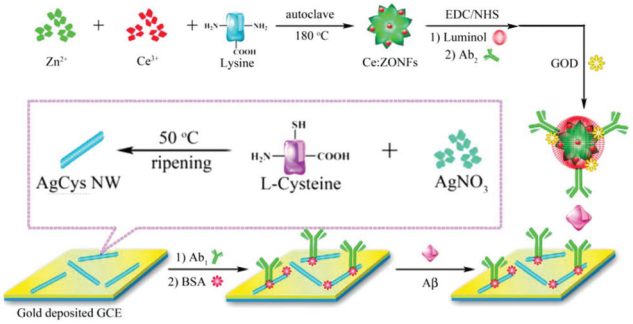

Fig. 14 Schematic illustration of synthesis process of Ab_2-GOD@Ce:ZONFs-Lum signal probe and preparation process of the AgCys Nanowires. (Reprinted with permission from ref. 75. Copyright 2016 American Chemical Society.)

Table 2 The different kinds of co-reaction accelerators in ECL ternary system

Co-reaction accelerator	Luminophore	Co-reactant	Ref.
Semicarbazide	CdTe QDs	$S_2O_8^{2-}$	104
Perylene derivatives	CdTe QDs	$S_2O_8^{2-}$	105
Hemin	PTCA	$S_2O_8^{2-}$	106
Aniline	PTCA	$S_2O_8^{2-}$	93
Isoreticular metal organic framework-3	CdTe QDs	$S_2O_8^{2-}$	107
$CoFe_2O_4$ MNPs	PTC-NH_2	$S_2O_8^{2-}$	108
Ag NPs	SnO_2 nanoflowers	$S_2O_8^{2-}$	109
Fe_3O_4–CeO_2	Ag NCs	$S_2O_8^{2-}$	110
Ag NPs and Fe–Fe_2O_3 NPs	PTPE	H_2O_2	111
TiO_2	Ag NCs	Dissolved O_2	112
Au–Ag–Pt heteronanostructures	Doxorubicin-luminol	Dissolved O_2	113
Pt nanomaterials	Rubrene	Dissolved O_2	114

was much lower than the other QDs-$S_2O_8^{2-}$ ECL system (Fig. 15).[76] And the possible ECL mechanism of this strategy has also been investigated. This new strategy provides a new orientation for signal amplification in ECL biosensing.

2.1.3.3 Signal-on induced by ECL-RET. ECL-RET is one of the high-efficiency means to construct a signal-on mode ECL biosensor. Up to now, abundant ECL-RET systems such as luminol-Ru,[18] luminol-QDs,[12] and QDs-Ru[77] have been put forward and applied in many fields. In an ECL signal-on mode, the donor is always introduced in a detection solution where acceptor had existed before. Ju's group used luminescent conjugated polymer as a carrier to synthesize $Ru(bpy)_3^{2+}$-doped polymer dots (RuPdots). What's more, it was demonstrated that the resonance energy transferred from the excited polymer dots to the encapsulated $Ru(bpy)_3^{2+}$ led to a 15.7-fold higher ECL emission than that of $Ru(bpy)_3^{2+}$ with the same amount at the gold electrode (Fig. 16).[78] It achieved a detection limit of 0.8 fM using mutant KRAS gene as a model target.

2.1.3.4 Signal-on induced by nucleic acid amplified strategy. With the development of nucleic acid technology, some nucleic acids amplified strategies have been developed for bio-

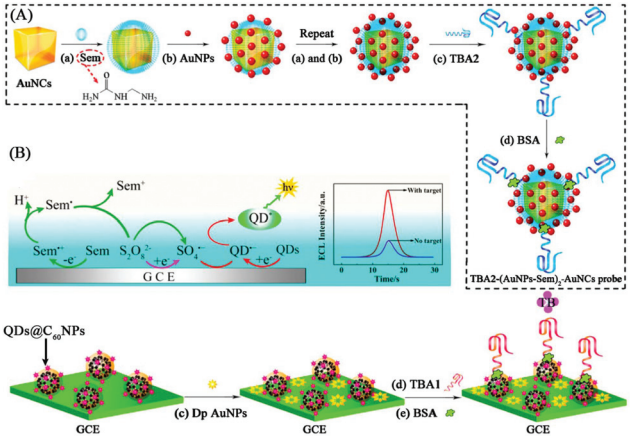

Fig. 15 Schematic illustration of ECL aptasensor preparation process and possible luminescence mechanism: (A) fabrication of TBA_2-(AuNPs-Sem)$_n$-AuNCs signal probe; (B) fabrication of CdTe QDs@C60 NPs, and (C) possible ECL mechanism of the QD-based ECL system. (Reprinted with permission from ref. 77. Copyright 2015 American Chemical Society.)

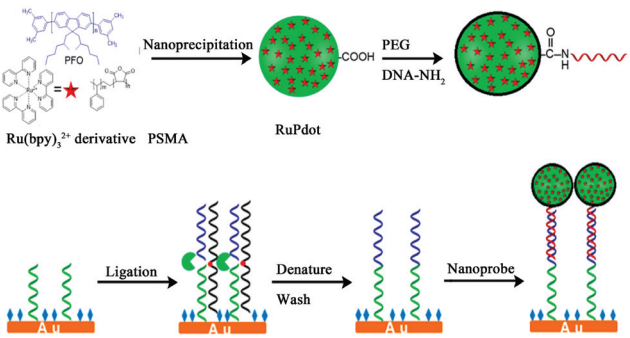

Fig. 16 Schematic diagrams of (A) Preparation of RuPdots nanoprobe using PFO, hydrophobic $Ru(bpy)_3^{2+}$ derivative, and PSMA; (B) SNP detection with ligase detection reaction and nanoprobe. (Reprinted with permission from ref. 78. Copyright 2017 American Chemical Society.)

sensor construction with targets of DNAs, microRNAs, and proteins.[79,80]

Among them, enzyme-free signal amplified strategies such as recycle hybridization chains reaction (HCR), strand displacement reaction (SDR), and catalyzed hairpin assembly (CHA) are utilized in ECL bioassays. Chen and co-workers have obtained sensitive DNA detection by HCR to efficiently intercalate $Ru(phen)_3^{2+}$ into grooves of the dsDNA polymers (Fig. 17).[81]

Compared with static nucleic acid based amplification strategy, DNA-based nanomachines, which could be transformed with external stimuli leading to cargoes transit and realizing targets detection, attracted much attention of researchers. Most DNA nanomachines performed under one-dimensional (1D) or two-dimensional (2D) tracks, which limited the capture of payloads to a certain degree and went against sensitivity improvement.[82] Recently, a few DNA nanomachines that performed on three-dimensional (3D) material have been reported due to the high DNA loading density on 3D material. Jiang and co-workers designed an ultrasensitive ECL signal-on a biosensor through target mucin 1 powered CHA which acted as 3D DNA nanomachine signal probe (Fig. 18).[83] The prepared ECL biosensor showed a favorable linear response for mucin 1 detection with a relatively low detection limit of 0.62 fg mL^{-1}.

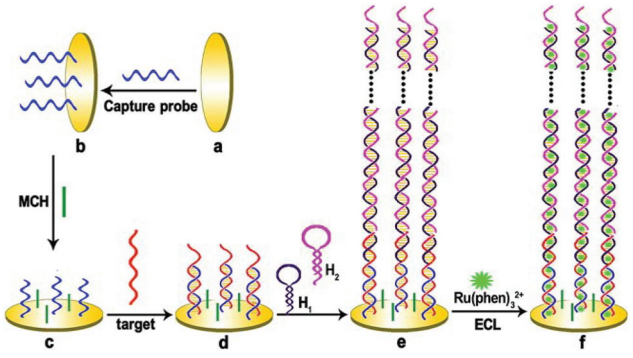

Fig. 17 Illustration of the universal and highly sensitive HCR-based strategy for ECL detection of DNA. (Reprinted with permission from ref. 81. Copyright 2012 American Chemical Society.)

2.2 Multiple signal switching mode

Despite the above advantages, single signal switching mode-based ECL biosensors may induce false negative or positive signals, which limits their application in analysis of real samples. Thus, a new intelligent output signal mode, named the multiple signal switching mode, has achieved extensive attention due to further improvements of selectivity and specificity. Usually, a multiple signal switching mode mainly includes the following four types: (i) signal off-on mode, (ii) signal on–off mode, (iii) signal on–off–on mode and (iv) ratiometric ECL biosensing.

2.2.1 Signal off–on mode. The signal off–on switch mode usually contains two steps. The first step is the initial "switch-

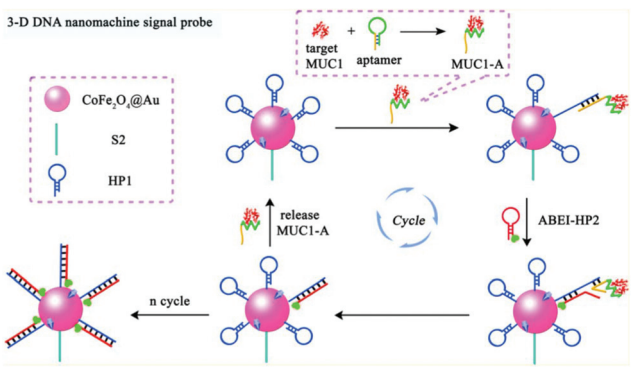

Fig. 18 Scheme of (A) Assembly process of 3-D DNA nanomachine signal probe induced by protein-aptamer binding complex; (B) Schematic diagrams of the construction and luminescence Reaction mechanism of the biosensor. (Reprinted with permission from ref. 83. Copyright 2017 American Chemical Society.)

off" state with a low ECL signal, which can be caused by introduction of a quencher probe to obtain a low background signal. The second step is the "switch-on" state, which can be achieved in the presence of the target by taking away the quencher probe to recover the ECL signal. The change of ECL intensity correlates to the concentrations of target. For proof of concept application, this signal off–on switch mode opens new opportunities for bioanalysis.[83–86] So far, there are many kinds of "off–on" switch biosensors that have been reported. For example, as shown in Fig. 19, Zhang *et al.* reported an off–on switching of a dual amplified ECL biosensor based on Pb^{2+}-induced DNAzyme-assisted target recycling and rolling circle amplification for microRNA detection. First, the "switch-off" state was obtained by the quenching effect of dopamine towards a luminol/H_2O_2 system owing to the DNA hybridization reaction of the dopamine modified DNA sequence (S1) with HP hairpin probe. The primer probe was incubated with the assistant probe and the target RNA to form a Y junction structure. Participation of Pb^{2+} cleaved the Y junction on the cleavage site, bringing about the release of the target and generating intermediate DNA (S2). Then the S2 was loaded onto the prepared electrode to displace S1 and served as an initiator for RCA, where numerous repeated DNA sequences coupling with hemin to form a hemin/G-quadruplex exhibited strongly catalytic behaviour toward H_2O_2, and thus amplified the ECL signal to obtain the second "switch-on" state.[87] More recently, Xiong *et al.* developed an "off–on" ECL biosensor for the determination of telomerase activity, which was obtained by using a self-enhanced ruthenium polyethylenimine (Ru-PEI) complex doped zeolitic imidazolate framework-8 with high ECL efficiency as an ECL indicator and an enzyme-assisted DNA cycle amplification strategy.[88]

2.2.2 Signal on–off mode. The signal on–off switch mode contains two steps. The first step is to construct the initial "switch-on" state with a high ECL signal by using signal amplification strategy. The second step is to achieve a "switch-off" state, which can be caused in the presence of the target by introduction of a quencher probe to obtain a low background signal. And then, the changes of ECL intensity correlate to the concentrations of target. For example, as shown in Fig. 20, Fan *et al.* reported an "on–off" ECL biosensor for concanavalin A (Con A) detection. The first "switch-on" state with strong ECL signal was obtained by an Ag-doped graphitic carbon nitride nanosheet (Ag–g-C_3N_4) modified glassy carbon electrode toward the $S_2O_8^{2-}/O_2$ system. As expected, in the presence of target Con A, the second "switch-off" state was achieved by the introduction of the quenching probe of polyaniline-3,4,9,10-perylenetetracarboxylic acid-DexP conjugate (denoted as PANI-PTCA-DexP).[89] Although the "on–off" switch mode is simple and convenient, there are still some drawbacks, such as a high background signal and relatively low sensitivity.

2.2.3 Signal on–off-on mode. Specifically, the "on–off–on" switch contains three steps. The first step is the initial "signal-on" state with a strong signal. The second step is the "switch-off" state caused by introduction of a quencher probe. The third step is a "switch-on" state, which can be achieved in the presence of the target by taking away the quencher probe. Compared to the "on–off" switch mode and "off–on" mode, this "on–off–on" switch strategy not only possess low background signal and high sensitivity, but also improves the specificity of analytical detection.[90,91] As shown in Fig. 21, we designed a label-free ECL aptasensor based on a novel "on–off–on" switch for highly sensitive determination of kanamycin. The first "switch on" state with remarkably high ECL intensity was obtained by a tri-layer composite film modified glassy carbon electrode towards the $S_2O_8^{2-}/O_2$ system. Later, the "switch-off" state was achieved by the quenching effect of hemin/G-quadruplex DNAzymes towards an $S_2O_8^{2-}/O_2$ system according to the DNA hybridization reaction of assistant probes (APs, guanine-rich nucleic acid) with capture probes

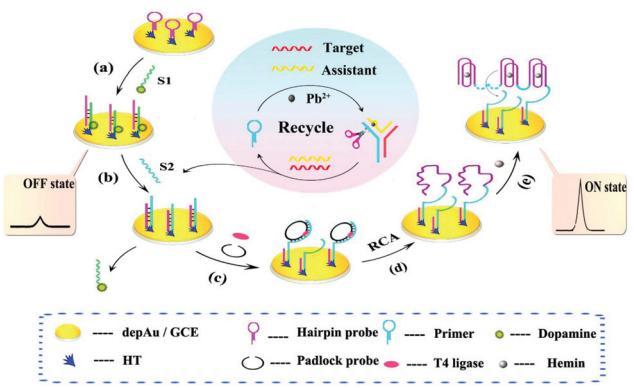

Fig. 19 Schematic diagram of the dual amplified assay: (a) modification of S1, (b) displacement of S1 by S2, (c) incubation of T4 ligase and padlock probe, (d) RCA process, and (e) the formation of Hemin/G-quadruplex. (Reprinted with permission from ref. 87. Copyright 2015, American Chemical Society.).

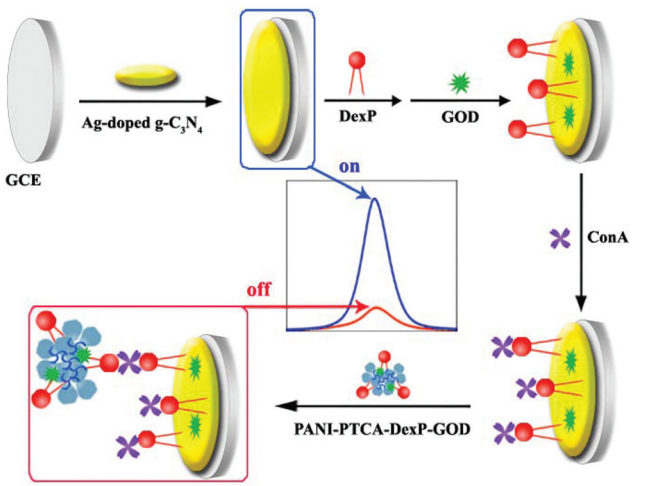

Fig. 20 The illustration of the synthetic process of (A) Ag–g-C_3N_4 and (B) PANI-PTCA-DexP-GOD, and (C) the preparation of the ECL biosensor. (Reprinted with permission from ref. 89. Copyright 2016, Elsevier.)

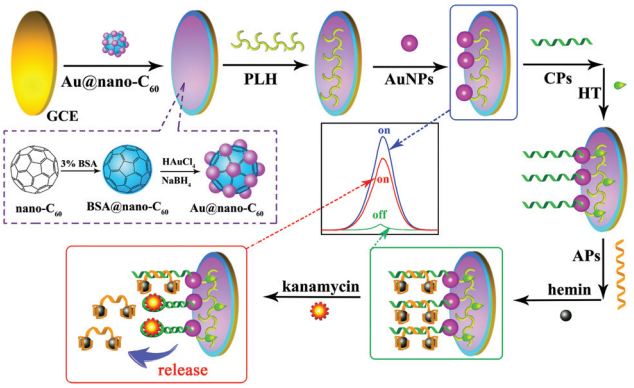

Fig. 21 Schematic diagram of the preparation of the ECL aptasensor. (Reprinted with permission from ref. 92. Copyright 2015, Elsevier.)

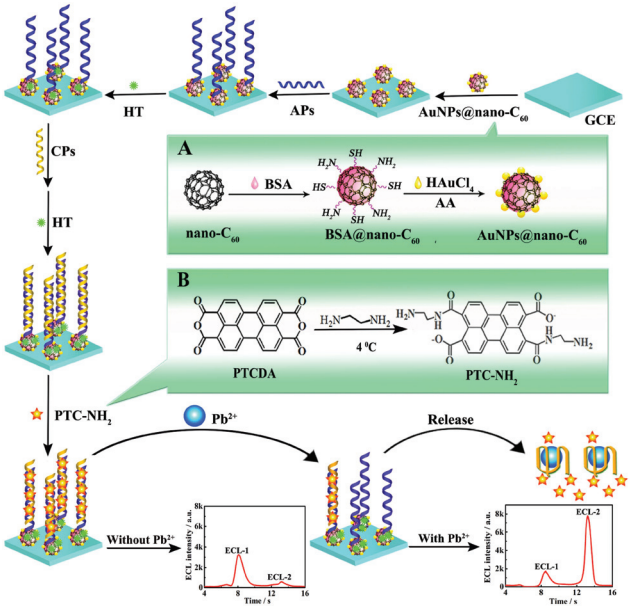

Fig. 22 Schematic illustration of the preparation process of the ratiometric aptasensor: inset of (A) and (B) display the preparation procedure of AuNPs@nano-C_{60} and PTC-NH_2. (Reprinted with permission from ref. 14. Copyright 2015, American Chemical Society.)

(CPs) which could generate a large amount of hemin/G-quadruplex DNAzymes in the presence of hemin with a simple and label-free process. As expected, the second "switch-on" state was the ECL signal recovery when the target of kanamycin was present and it was attributed to the formation of the aptamer-kanamycin complex which then made the quencher of hemin/G-quadruplex DNAzymes release from the sensing interface. This novel concept of the "on–off–on" switch system strategy was expanded to determine kanamycin in a dynamic range from 0.15 nM to 170 mm with a low detection limit of 45 pM.[92] Later, we also designed an "on–off–on" switch system for the highly sensitive and selective detection of Cu^{2+} by using ECL quencher probes (Fc-NH_2/Cu-Sub/Au NPs) in a PTCA/aniline/$S_2O_8^{2-}$ system.[93] In another example, inspired by the quenching effect of Hg^{2+} on the ECL response of ABEI, an ECL aptasensor based on the "on–off–on" signal switch strategy and target recycling amplification strategy was successfully developed for Hg^{2+} and mucin1 detection.[94]

2.2.4 Ratiometric ECL biosensing. The signal on–off–on switching mode is based on single emission intensity changes, which may exhibit false positive/negative errors during the detection process owing to instrumental efficiency or some environmental changes, such as a nontarget-induced reagent degradation/dissociation, the concentration of a co-reactant, pH, *etc*. To alleviate these interference factors, ratiometric ECL measurements were proposed in recent works, where quantification depends on the ratio changes of two emission intensities instead of absolute values, providing more precise results *via* normalizing most ambiguities by self-calibration.

Ratiometric measurements based on the ECL-RET between two emitters are extensively explored, and an ECL-RET often occurs between a suitably matched donor/acceptor pair. For example, Ju *et al.* designed a dual-potential ratiometric ECL sensing approach for Mg^{2+} detection *via* ECL-RET between CdS QDs and Cy5 molecules.[95] As shown in Fig. 22, we reported a ratiometric aptasensor for Pb^{2+} detection based on the ECL-RET from O_2/$S_2O_8^{2-}$ to a kind of amino-terminated perylene derivative (PTC-NH_2). The ECL dual peaks at −0.7 V and −2.0 V were obtained when the prepared aptasensor was detected in an air-saturated $S_2O_8^{2-}$ solution, which could be attributed to the emission of excited dimmers (π-excimers) ($^1(NH_2\text{-PTC})_2$*) and $^1(O_2)_2$*, respectively. In the presence of Pb^{2+}, the dsDNA was unwound, and a Pb^{2+} G-quadruplex structure generated because of the highly specific affinity between Pb^{2+} and CPs, which made PTC-NH_2 release from the electrode surface. As a result, the ECL signal at −0.7 V was decreased, and the ECL signal around −2.0 V was increased. By measuring the ratio of ECL intensities at two excitation potentials, the developed aptasensor exhibited a high selectivity for Pb^{2+} detection.[14] Later, Wei's group fabricated a ratiometric biosensor for trinitrotoluene (TNT) detection, where an effective ECL-RET was achieved from luminol (donor) to CdTe QDs (acceptor).[96] In addition, in order to further extend the field of ratiometric ECL-RET system applications, Xu' group recently reported a dual-wavelength ratiometric approach for miRNA detection, where ECL-RET from a graphite-like carbon nitride nanosheet (g-C_3N_4 NS) to $Ru(bpy)_3^{2+}$ resulted in one emission peak.[97]

It should be noted that the occurrence of ECL-RET needs to search for a suitable donor–acceptor pair, which greatly limits practical applications of ratiometric assays. Therefore, metal nanomaterials have been extensively employed to enhance or quench ECL intensity *via* RET, a surface plasmon resonance or catalysis effect in two different emitters systems, and thus construct a series of dual-potential ratiometric ECL biosensors such as Pt NPs,[98] Au NPs,[99,100] gold nanorods (AuNRs),[101] Ag NPs,[102] and Cu_2O nanocrystals.[103] As shown in Fig. 23,

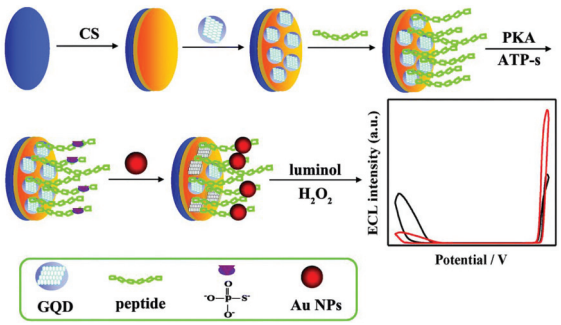

Fig. 23 (A) Illustration of the ECL ratiometric approach for monitoring PKA activity and inhibitor screening. (Reprinted with permission from ref. 116. Copyright 2016, Royal Chemical Society.)

Zhao *et al.* developed an Au NPs mediated dual-potential ECL ratiometric approach for highly sensitive protein kinase activity and inhibition assay based on the simultaneous decrease of cathodic ECL from graphene quantum dots (GQDs) and enhancement of anodic ECL from luminol.[115] Later, Huang *et al.* proposed a novel co-reactant-dependent ratiometric ECL method with luminol and CdS QDs as ECL emitters on the basis of the high catalytic ability of Pd NCs towards hydrogen peroxide as a co-reactant.[116]

Enzymes and metal ions are also employed to enhance or quench ECL intensity and construct double-potential ratiometric ECL without the ECL-RET. As shown in Fig. 24, we explored a double-potential ratiometric approach for organophosphorus pesticides (OPs) analysis, where the reduced graphene oxide-CdTe QDs and carboxyl conjugated polymer dots (PFO dots) were chosen as cathodic and anodic ECL emitters, and dissolved O_2 and the product (H_2O_2) from enzymatic reactions served as their co-reactants, respectively.[117] Meanwhile,

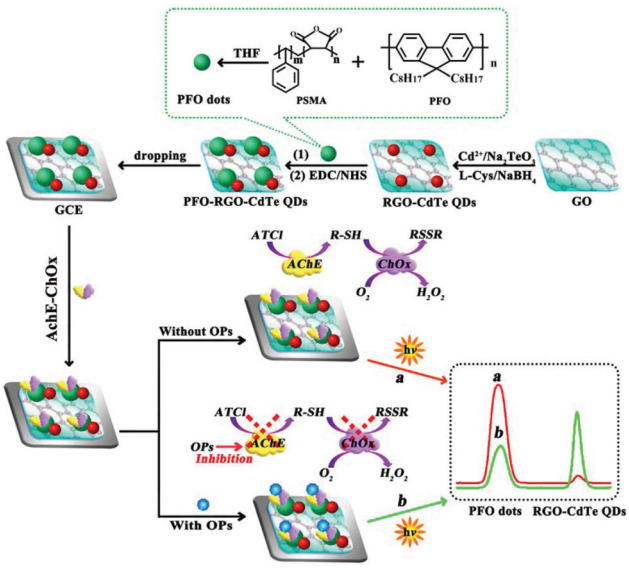

Fig. 24 Double-potential ratiometric ECL for organophosphorus pesticides (OPs) analysis. (Reprinted with permission from ref. 117. Copyright 2017, American Chemical Society.)

Jiang *et al.* reported a novel ratiometric ECL strategy combination of dual-potential ECL signals from Au–g-C_3N_4 nanocomposites and luminol dependent on *in situ* generation and conversion of co-reactants initiated by catalytic reactions of glucose oxidase (GOx) for glucose detection.[118] In addition, Liu's group reported that the double-potential ECL signals could be actuated by different ECL reactions merely from graphite-phase polymeric carbon nitride (GPPCN) nanosheets at anodic and cathodic potentials, respectively, where the different metal ions exhibited distinct quenching/enhancement of the ECL signal at different driven potentials.[119] Later, Yao's group developed a single luminophore dual-potential ratiometric ECL system for Co^{2+} detection, where the Co^{2+} could evidently amplify the anodic intensity and quench the cathodic ECL intensity.[120]

The dual-responses of an electrochemical and ECL ratiometric approach was reported at different potentials, which could alleviate cross-talking response. As shown in Fig. 25, Wu's group also developed dual-responses of an electrochemical and ECL ratiometric aptasensor for aflatoxin B1 (AFB1) detection. The electrochemical method was first used as a model to verify the specific interaction between AFB1 and the aptamer, in which Fc-anchored and methylene blue (MB)-anchored DNA sequences acted as dual signal producers. Consequently, the specific interaction between AFB1 and its aptamer was demonstrated by the "signal-on" mode of Fc and the "signal-off" mode of MB. Due to the dual-signal mode, the electrochemical sensor was further extended to the construction of an ECL aptasensor. In the ECL system, dual ECL signals were produced from CdTe/CdS/ZnS quantum dots (QDs) and luminol. Horseradish peroxidase-modified gold nanorods (HRP/Au NRs) acted as the quencher/enhancer and as such quenched the ECL signal of the QDs by ECL energy transfer and simultaneously catalyzed H_2O_2 to enhance the ECL of luminol. Owing to the self-calibration from the internal reference, both of the ratiometric aptasensors exhibited accurate and sensitive analytical performance for AFB1 detection.[121] Jiang *et al.* also reported a ratiometric biosensor on a screen-printed carbon electrode (SPCE) for multiplexed detection of miRNAs based on the ratio of ECL intensity to cyclic voltammetry (CV) current.[122]

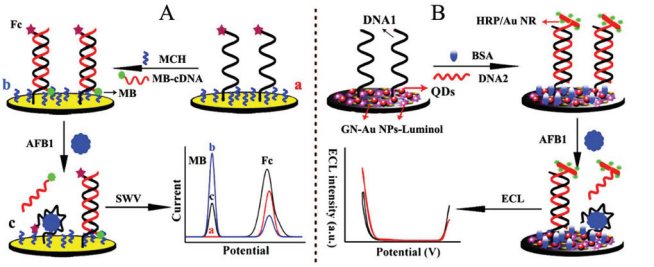

Fig. 25 Schematic illustration of the dual-signaling sensor for AFB1 assay with (A) electrochemistry and (B) electrochemiluminescence. (Reprinted with permission from ref. 121. Copyright 2017, American Chemical Society.)

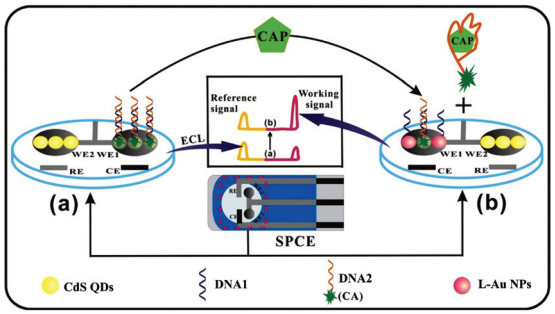

Fig. 26 Schematic illustration of the ratiometric ECL array for CAP quantification. (Reprinted with permission from ref. 89. Copyright 2015, Elsevier.)

The above-mentioned ratiometric ECL measurements adopt one working electrode modified by two emitters, which remains a challenge to choose the emitters and balance their ECL excitation potentials, intensities, wavelengths and co-reactants. In addition, the applied optical filters for these approaches could decrease the ECL intensity. Remarkably, a spatial-resolved ratiometric ECL approach based on a bipolar electrode for bioanalysis is simpler and more sensitive since the two ECL reactions can be spatially separated and no optical filters are required for data acquisition. As shown in Fig. 26, Feng *et al.* fabricated a ratiometric ECL aptasensor array on one homemade screen-printed carbon electrode (SPCE) substance consisting of two spatially resolved working electrodes to detect antibiotic chloramphenicol (CAP) based on the ratio of the working signal to the internal reference signal.[123] Chen's group also developed a closed bipolar electrode (BPE)-ECL device for ratiometric detection of prostate specific antigen (PSA).[124]

2.3 ECL imaging mode

Although ECL analysis utilizes a photomultiplier tube (PMT) to achieve high sensitivity and a low detection limit, this method is not applicable to a complicated detecting system and also lacks ability for high-throughput analysis.[125,126] Recently, ECL imaging has emerged as a novel technique in the ECL field; it uses a charge coupled device (CCD), or even naked eyes, instead of a PMT to image the ECL phenomenon and achieves simultaneous visual detection without the use of complicated detection systems and time-consuming data processing.[127] In addition, ECL imaging offers remarkable superiorities over the widely used fluorescence and chemiluminescence imaging techniques in terms of minimized interruption of background light and improved spatial resolution, respectively.[128] Therefore, the ECL imaging technique has been extensively investigated and applied in various areas, including microfluidic systems with bipolar electrodes (BPE),[129,130] latent fingerprints (LFPs) visualization,[131,132] immunoassay microarray,[133] and metabolic toxicity screening.[134,135]

Generally speaking, the previous work on ECL imaging is carried out for high-throughput analysis based on ECL arrays in microfluidic system. A bipolar electrode (BPE) combined with an ECL imaging technique is usually established in microfluidic chips, which can be used as an imaging tool to investigate biological recognition events. BPE-ECL imaging can be performed in two separated solutions (closed BPE) or one solution (open BPE). Wu *et al.* fabricated an ECL imaging platform for simultaneous detection of cancer biomarkers based on a closed BPE array. Multiple cancer biomarkers can be accurately quantified using an antibody/aptamer-based assay and doping thionine in silica nanoparticles coupled nanobioprobes activated ECL reaction on specific BPEs.[129] As shown in Fig. 27, Zhang *et al.* developed a visual ECL sensing platform based on a dual-bipolar electrode (D-BPE) array chip. The chip was composed of two arrays of BPEs and three separated arrays of reservoirs filled with buffer, $Ru(bpy)_3^{2+}$-TPrA, and luminol solutions, respectively. Both BPEs served as ECL reporting platforms. By applying 6.0 V voltage, an array of orange ECL signals belonging to $Ru(bpy)_3^{2+}$ turned on. After adding DNAzyme and H_2O_2 in $Ru(bpy)_3^{2+}$ and luminol reservoirs, the orange $Ru(bpy)_3^{2+}$ signals decreased until they vanished due to the quenching effect. Meanwhile, a new array of blue ECL signals turned on because of the luminol-H_2O_2 ECL reaction. The designed D-BPE had superior properties compared with the three-electrode system and benefitted from the quantitative relation of the bipolar systems, which greatly enhanced the ECL detection sensitivity. Meanwhile, the visual color-switch ECL and the ratiometric detecting principle made the results easier to evaluate and more accurate. These designed and fabricated D-BPE ITO chips give different colors of ECL signals for human promyelocytic leukemia (HL-60) cancer cells detection.[136] In addition, open BPE-ECL imaging has also been studied. Liu *et al.* developed a paper-based open BPE-ECL imaging sensing for visual detection.[137] Later, Liu and coworkers also reported a battery-triggered open wireless ECL sensing strategy based on microfluidic cloth-based bipolar devices for measurements of H_2O_2 in milk and glucose in clinical urine and serum samples.[138]

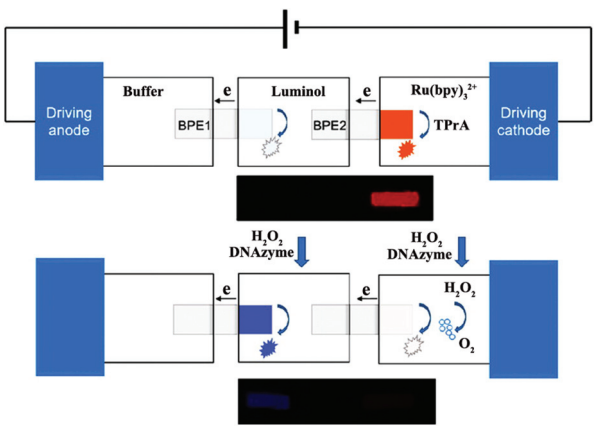

Fig. 27 (A) Structure of double-bipolar electrodes (D-BPE), operation procedures of BPE-ECL sensing platform and ECL image of D-BPE. (Reprinted with permission from ref. 136. Copyright 2014, American Chemical Society.)

Fingerprints are rarely seen (termed latent fingerprints, LFPs), but this methodology has been established as one effective trace that can be used as important evidence for an individual's identification.[139,140] The ECL imaging technique can be used as an effective means to enhance the visualization of LFPs. As shown in Fig. 28, Xu and co-workers presented the combination of ECL imaging with enzyme immunoassay for the highly sensitive detection of protein/polypeptide residues in latent fingerprints. The single-HRP route was established to exemplify the fingerprint visualization approach using human immunoglobulin G (hIgG) as a test protein. Then, a multiple-HRP route further improved it and was applied for highly sensitive detection of the trace residues, *i.e.*, epidermal growth factor, lysozymes, and dermcidins that are excreted by human eccrine glands.[141] Su's group also exploited two operating methods for visualizing LFPs on the basis of spatially selective control of ECL generation at the electrode surface.[142] Later, Tan *et al.* established an image-contrast technology based on the intrinsic mechanism of the ECL dynamic process for visualizing LFPs and *in situ* detection of TNT in fingerprints.[143]

The ECL imaging technique also has been widely used in clinical diagnostic immunoassays, which show some obvious advantages, such as rapid analysis, multi-component detection, and visualization. As shown in Fig. 29, Deiss *et al.* fabricated a class of sensing microarray that utilized ECL as a readout mechanism to detect multiple antigens simultaneously. The approach involved attaching specific receptors to microbeads and lead to localization of all the ECL reagents on the microbeads where the analyte had bound.[144] Xu and co-workers fabricated an ECL immunosensor array featuring capture-antibody-decorated single-wall carbon nanotube forests residing in the bottoms of 10 μL wells with hydrophobic polymer walls. Silica nanoparticles containing Ru $(bpy)_3^{2+}$ and secondary antibodies were employed in this system for highly sensitive two-analyte detection.[145] Later, Sentic *et al.* reported that ECL imaging resolved at the single bead level provided a general description of the ECL phenomena operating in a bead-based ECL immunoassay, which allowed the deciphering of the mechanistic route, testing of co-reactant efficiency, and visualisation of the associated optical focusing effects.[146]

Toxicity assessment is a major problem in drug and environmental chemical development. Toxicity screening was also achieved by using ECL arrays in recent years. As shown in Fig. 30, Hvastkovs *et al.* presented and validated an ECL array format suitable for genotoxicity screening of compounds metabolized by cytochrome P450 (cyt P450, or CYP) and other

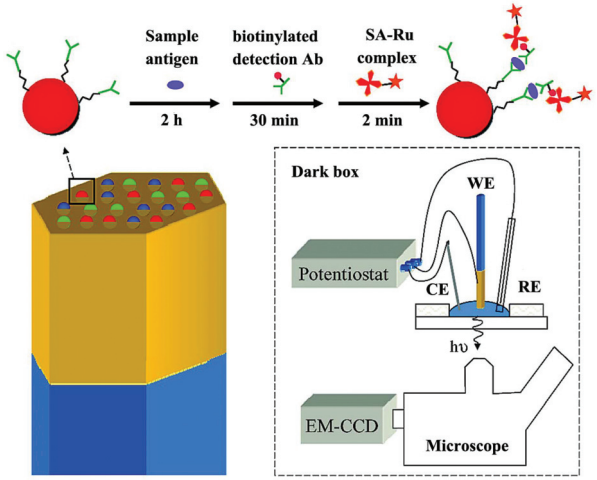

Fig. 29 (Top) A sandwich immunoassay is performed by exposing antibody-functionalized microbeads to three solutions. The beads are housed in microwells created from an etched gold-coated fiber-optic bundle. The gold coated fiber bundle acts as the working electrode (WE) for ECL. CE and RE refer to counter electrode and reference electrode. (Reprinted with permission from ref. 144. Copyright 2009, American Chemical Society.)

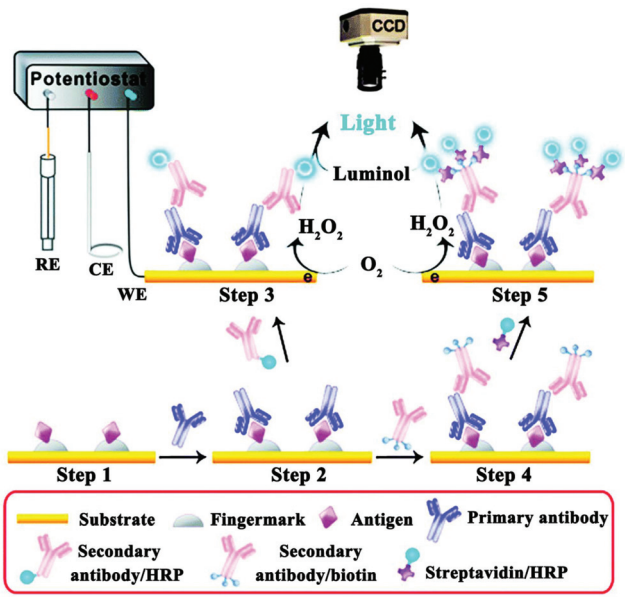

Fig. 28 Illustration of the detection of antigenic residues present in a fingerprint using enzyme immunoassay and ECL imaging. (Reprinted with permission from ref. 141. Copyright 2014, Royal Society Chemistry.)

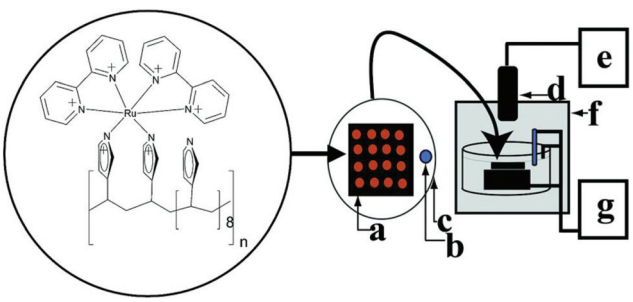

Fig. 30 Conceptual diagram of the ECL array instrumentation. RuPVP polymer, DNA, and enzymes are located at each spot on a (a) pyrolytic graphite block; with (b) Ag/AgCl reference electrode, (c) Pt wire counter electrode, (d) CCD camera, (e) computer, (f) gel-doc dark room, and (g) potentiostat for applied voltage control. (Reprinted with permission from ref. 147. Copyright 2007, American Chemical Society.)

enzymes, and which also can assign relative genotoxic activity to specific enzymes. Array spots containing DNA, various human cyt P450s, and ECL generating metallopolymer $[Ru(bpy)_2PVP_{10}]^{2+}$ were exposed to H_2O_2 to activate the enzymes. ECL from all spots was visualized simultaneously using a CCD camera. Using benzo[*a*]pyrene as a test substrate, enzyme activity for producing DNA damage in the arrays was found in the order CYP 1B1 > CYP 1A2 > CYP 1A1 > CYP 2E1 > myoglobin, which is the same as the order of their metabolic activity. Thus, these arrays estimated the relative propensity of different enzymes to produce genotoxic metabolites.[134] Pan *et al.* presented a metabolically representative ECL array by testing 11 chemicals of varying toxicity and exploring correlations with rodent toxic dose (TD50) and lethal dose (LD50), Ames tests, and Comet assays.[147] Later, Wasalathanthri *et al.* described a comprehensive approach to evaluate chemical genotoxicity pathways from metabolites formed *in situ* by a broad spectrum of liver, lung, kidney and intestinal enzymes.[148]

Overall, ECL imaging is quite applicable to a complicated detecting system for high-throughput analysis and exhibits many advantages such as low background signal, simple instrumentation required, high sensitivity, low background signal, and high controllability. However, there still exist many unresolved problems and challenges. For example, the most prominent thing is that the sensitivity of imaging was not efficient enough because many ECL systems with a relatively low intensity could not achieve an image with high resolution. Therefore, future studies should be performed toward improving ECL efficiency of luminophores and constructing advanced imaging devices suitable for both electrochemical stimulation and light harvesting.

3. Combination of various signal output modes for multi-target detection on a single interface

In a clinical diagnosis, the detection of single target is not sensitive and specific enough to meet strict diagnostic criteria,[144,149–151] since pathogenesis is an intricate process and most diseases have multiple markers associated with their incidence. Therefore, multi-target detection is becoming increasingly significant for early cancer screening and diagnosis. Based on the unique properties of ECL, such as the high sensitivity, wide detection range, and short time consumption. ECL technology has shown great potential for multi-target detection. However, it is necessary to consider the inevitable cross reactions between different ECL luminophores in the same ECL system, which directly interferes with the accurate detection of different targets.

Recently, substantial works have been devoted to multiple target determinations based on a potential-resolved ECL sensing platform with multiple ECL luminophores.[144,152] Han *et al.* constructed a potential resolved multiplex ECL sensing platform for the quantification of AFP and CEA antigen at cells using $Ru(bpy)_3^{2+}$ and luminol as ECL probes.[153] In this work, a self-quenching of luminescence was initialized by the introduction of concentrated aqueous luminol to obtain accurate measurements of two potential-resolved ECL signals from $Ru(bpy)_3^{2+}$ and luminol. Furthermore, Yang's group designed a mutiplex cytosensor based on a dual ECL signal system for simultaneous and *in situ* evaluation of the expression levels of mannose and epidermal growth factor receptor (EGFR) on MCF-7 cell surfaces.[154] As shown in Fig. 31, a more facile device based on an ITO electrode with two spatially resolved areas spaced 3 mm apart was designed to exclude the interference between Au@luminol and CdS QDs covalently linked with concanavalin A (ConA) and epidermal growth factor (EGF), respectively. Furthermore, this multiplex biosensor was applied for simultaneous quantitative evaluation of the expression levels of mannose and EGFR on MCF-7 cells, which is expected to develop a better diagnostic tool for diseases.

However, the above mentioned traditional strategies for multiple ECL detection employed different ECL probes, where cross-reactivity between ECL probes in multiplex detection existed. Recently, Yuan's group adopted multiple signal output modes to realize different biomarkers detection with a single luminophore.[155] Therein, multiple sensitive detection of the miRNA biomarkers was performed by the introduction of dual miRNAs-fueled DNA nanogears into an enzyme-free ECL biosensor. In this work, the ECL "signal-on" or "signal-off" depended on the movement of the DNA nanogears driven by different target miRNAs, which changed the distance of QDs and AuNPs to obtain different ECL signals (Fig. 32). Similarly, Peng *et al.* designed a DNA walker induced by dual miRNAs of miRNA-21 and miRNA-155 to construct an ECL biosensor by using CdS:Mn NCs as the ECL emitters.[156] Interestingly, the DNA walker could migrate along the track and then return to the original position, which made the proposed biosensor regenerated.

Over the years, numerous studies indicate that the detection of different kinds of biomarkers could reflect more comprehensive information and play decisive roles in clinical diag-

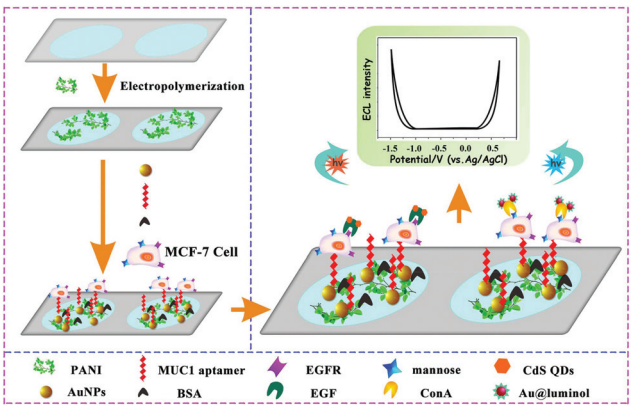

Fig. 31 Preparation and Schematic Illustration of the Dual Electrochemiluminescence Signal System. (Reprinted with permission from ref. 154. Copyright 2017 American Chemical Society.)

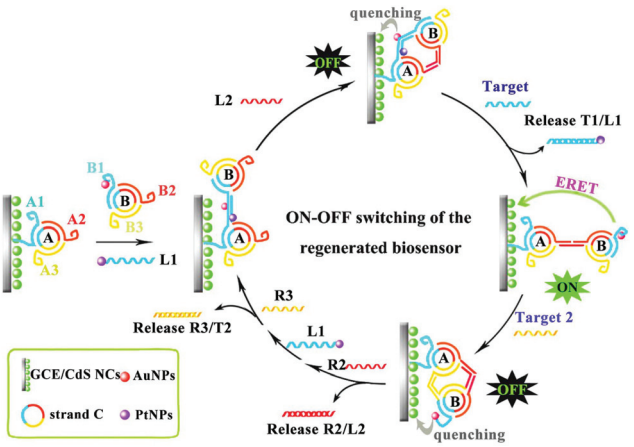

Fig. 32 Operating principle of the dual miRNAs-fueled nanogear-based regenerated biosensor which realized the multiple ECL detection of miRNAs with a single luminophore. (Reprinted with permission from ref. 155. Copyright 2017 American Chemical Society.)

nosis. Nie *et al.* reported a "on–off–on" switching platform to construct an ultrasensitive ECL biosensor for the detection of miRNA-141 and matrix metalloproteinase-2 (MMP-2).[157] As shown in Fig. 33, based on a TdT-mediated extension and target induced cleavage of peptide, the ECL biosensor could successfully realize the sensitive detection of miRNA-141 and MMP-2 by varying ECL intensity of the different modification processes.

Although the above works achieved the dual component detection stepwise, it is an urgent challenge to develop a feasible strategy for simultaneous detection of multiple biomarkers on a single interface. Recently, Yuan's group proposed a simultaneous ECL assay to realize multiple detection of biomarker proteins on a single interface by a multivariate linear algebraic equation.[158] Based on the hybridization chain reaction (HCR) and rolling circle amplification (RCA) strategy, the proposed simultaneous ECL assay achieved a sensitive detection of the N-terminal of the prohormone brain natriuretic peptide (BNPT) and cardiac troponin I (cTnI) with satisfactory accuracy, which provided a new avenue for early disease diagnosis (Fig. 34).

By converting different proteins to partially coincident sequences, Liang *et al.* proposed a competitive method based ECL assay with a single ECL indicator for the first time to efficiently estimate the concentration ratio of two proteins, which overcame the limitations of simultaneous ECL *via* multiple ECL indicators with inevitable cross reactions.[159] As shown in Fig. 35, by converting P-gp and GAPDH to partially coincident nucleotide sequences, the concentration ratio between these different proteins was obtained to relate ECL signals *via* a sandwich type immunoassay on magnetic beads based on competitive nucleotide hybridization on an electrode surface. In order to amplify the responses, rolling circle amplification (RCA) was employed to produce repeated nucleotide sequences, which was enzymatically cut into different partially coincident nucleotide sequences to competitively react with the captured nucleotide sequences modified on the electrode surface. Especially, one of these partially coincident nucleotide sequences could capture the signal probes. Thus, ECL signals could be employed to demonstrate the competitive reactions and the concentration ratios of these nucleotide sequences which related to the target proteins.

Recently, self-powered sensors[160] for detection without external power sources has received increasing attention, owing to the excellent capability of a simple operation, miniaturization, and low-cost. Since Whitesides and co-workers[161]

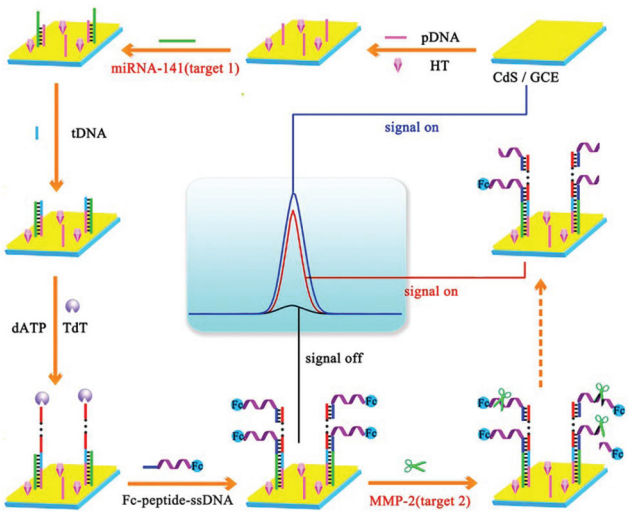

Fig. 33 Fabrication of an ECL biosensing platform for the detection of multiple types of biomarkers on a single interface. (Reprinted with permission from ref. 157. Copyright 2017 American Chemical Society.)

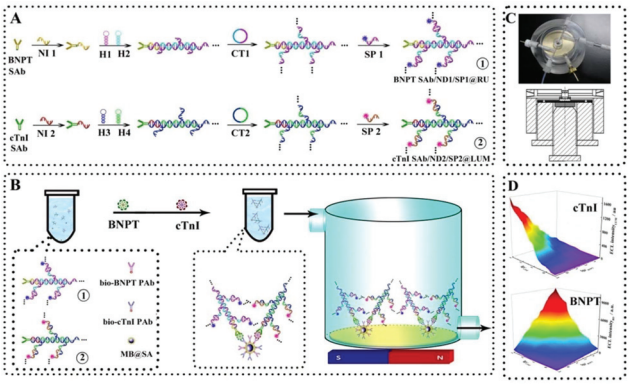

Fig. 34 Schematic diagrams of a simultaneous ECL assay: (A) preparation of the nucleotide dendrimer labeled secondary antibodies; (B) schematic diagrams of the simultaneous ECL assay system; (C) image and mechanical design drawing of self-designed magnetic flow system; (D) cathodic ECL responses of the as proposed ECL assay for multiple detection of BNPT and cTnI. (Abbreviations, bio-PAb, biotinylated primary antibody; CT1–2, circular template for RCA reaction; H1–4, hairpin nucleotide for HCR reaction; NI1–2, nucleotide initiator; SP1–2, signal probe). (Reprinted with permission from ref. 158. Copyright 2016 American Chemical Society.)

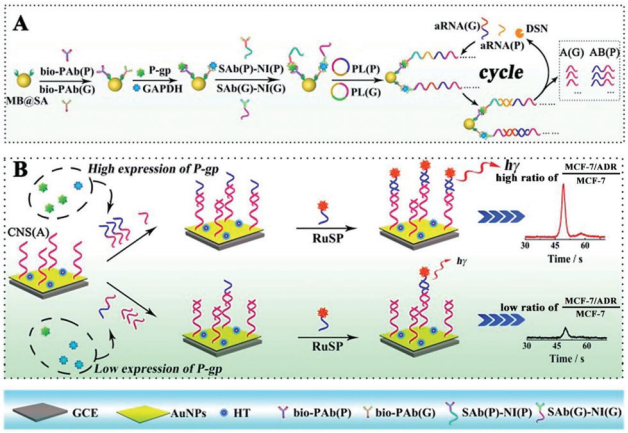

Fig. 35 Schematic diagrams of the competitive method-based ECL assay to demonstrate the concentration ratio of P-gp and GAPDH as a model. (A) Schematic diagrams of the sandwich type immunoassay on magnetic beads to convert the different proteins to partially coincident nucleotide sequences; (B) schematic diagrams of the competitive reaction on the sensor's surface to obtain the concentration ratio related ECL signals. (Reprinted with permission from ref. 159. Copyright 2016 The Royal Society of Chemistry.)

developed the paper-based analytical devices (μ-PADs), the rapid detection in clinical cancer screening and early diagnostic applications for remote regions and developing countries has moved a step closer to a simple, portable, disposable, and low-cost diagnosis. As a powerful analytical technique, ECL with excellent controllability, high sensitivity, and low-cost instruments has been widely applied in μ-PADs.[162–164] As shown in Fig. 36, Wang's group[165] developed a self-powered 3D origami microfluidic ECL biosensing device (μ-s-OECLD) for the very first time, which integrated with a noble metal-free and environmentally-friendly primary battery to measure the concentration of glucose from 0.1 mM to 3 mM (R = 0.9954) with a detection limit of 0.1 mM. Therefore, this simple, low-cost and disposable μ-s-OECLD exhibited great application potential for the detection of glucose in clinical diagnostics.

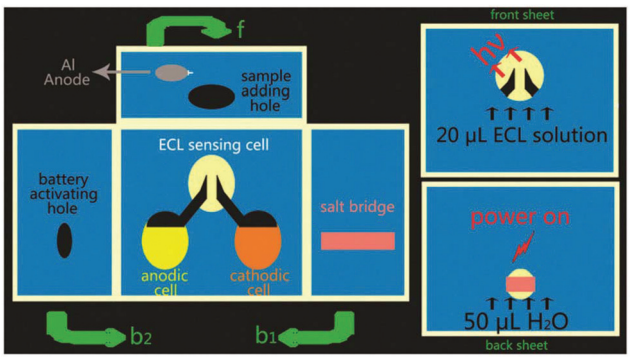

Fig. 36 Schematic diagram of the working principle of a m-s-OECLD. f: Front sheet; b1: the sheet folded to the back first; b2: the back sheet. (Reprinted with permission from ref. 165. Copyright 2013 The Royal Society of Chemistry.)

4. Conclusions and outlooks

Rapid improvements of ECL in both theoretical and practical areas have strongly proved that ECL is a significant method for the ultrasensitive determination of biomolecules. In this review, we have the retrospect of principles and advantages of applications of ECL based on different switching modes. Besides, we have focused the imaging studies in the ECL field. With the rapid developing of ECL analysis, the inherent virtues of ECL opens a new chapter in bioanalysis and other applications. We envision that the long-term needs in sensing, clinical diagnosis, biomedicine, food and environmental monitoring will continuously push the development of ECL analytical technology forwards.

Conflicts of interest

There are no conflicts to declare.

Acknowledgements

This work was financially supported by the NNSF of China (21775124, 21675129, 21675130 and 21575116) and Fundamental Research Funds for the Central Universities (XDJK2018AA003).

Notes and references

1 S. Y. Deng, J. P. Lei, Y. Liu, Y. Huang and H. X. Ju, *Chem. Commun.*, 2013, **49**, 2106–2108.
2 X. J. Li, Z. K. Guo, J. X. Li, Y. Zhang, H. M. Ma, X. H. Pang, B. Du and Q. Wei, *Anal. Chem.*, 2015, **854**, 40–46.
3 L. L. Liu, Q. Ma, Y. Li, Z. P. Liu and X. G. Su, *Biosens. Bioelectron.*, 2015, **63**, 519–524.
4 P. Zhao, L. F. Zhou, Z. Nie, X. H. Xu, W. Li, Y. Huang, K. Y. He and S. Z. Yao, *Anal. Chem.*, 2013, **85**, 6279–6286.
5 X. Y. Wang, P. Dong, W. Yun, Y. Xu, P. G. He and Y. Z. Fang, *Biosens. Bioelectron.*, 2009, **24**, 3288–3292.
6 W. Cao, J. Ferrance, J. Demas and J. P. Landers, *J. Am. Chem. Soc.*, 2006, **128**, 7572–7578.
7 A. E. Radi, J. L. A. Sánchez, E. Baldrich and C. K. Sullivan, *J. Am. Chem. Soc.*, 2006, **128**, 117–124.
8 J. Wang, Y. Shan, W. W. Zhao, J. J. Xu and H. Y. Chen, *Anal. Chem.*, 2011, **83**, 4004–4011.
9 M. Zhao, N. Liao, Y. Zhuo, Y. Q. Chai, J. P. Wang and R. Yuan, *Anal. Chem.*, 2015, **87**, 7602–7609.
10 P. Wu, X. D. Hou, J. J. Xu and H. Y. Chen, *Chem. Rev.*, 2014, **114**, 11027–11059.
11 M. S. Wu, H. W. Shi, J. J. Xu and H. Y. Chen, *Chem. Commun.*, 2011, **47**, 7752–7754.
12 Y. P. Dong, T. T. Gao, Y. Zhou and J. J. Zhu, *Anal. Chem.*, 2014, **86**, 11373–11379.
13 M. S. Wu, L. J. He, J. J. Xu and H. Y. Chen, *Anal. Chem.*, 2014, **86**, 4559–4565.

14 Y. M. Lei, W. X. Huang, M. Zhao, Y. Q. Chai, R. Yuan and Y. Zhuo, *Anal. Chem.*, 2015, **87**, 7787–7794.
15 Y. P. Dong, Y. Zhou, J. Wang and J. J. Zhu, *Anal. Chem.*, 2016, **88**, 5469–5475.
16 Y. P. Dong, Y. Zhou, J. Wang and J. J. Zhu, *Sens. Actuators, B*, 2016, **226**, 444–449.
17 J. Liu, M. Cui, H. Zhou and S. Zhang, *Sci. Rep.*, 2016, **6**, 30577.
18 J. L. Liu, M. Zhao, Y. Zhuo, Y. Q. Chai and R. Yuan, *Chem. – Eur. J.*, 2017, **23**, 1853–1859.
19 M. S. Wu, H. W. Shi, J. J. Xu and H. Y. Chen, *Chem. Commun.*, 2011, **47**, 7752–7754.
20 Q. M. Feng, Y. Z. Shen, M. X. Li, Z. L. Zhang, W. Zhao, J. J. Xu and H. Y. Chen, *Anal. Chem.*, 2015, **88**, 937–944.
21 M. S. Wu, H. W. Shi, L. J. He, J. J. Xu and H. Y. Chen, *Anal. Chem.*, 2012, **84**, 4207–4213.
22 Y. Cheng, Y. Huang, J. Lei, L. Zhang and H. Ju, *Anal. Chem.*, 2014, **86**, 5158–5163.
23 Z. Li, Z. Lin, X. Wu, H. Chen, Y. Chai and R. Yuan, *Anal. Chem.*, 2017, **89**, 6029–6035.
24 Y. Y. Zhang, Q. M. Feng, J. J. Xu and H. Y. Chen, *ACS Appl. Mater. Interfaces*, 2015, **7**, 26307–26314.
25 J. Wang, Y. Shan, W. Zhao, J. Xu and H. Chen, *Anal. Chem.*, 2011, **83**, 4004–4011.
26 M. M. Chen, Y. Wang, S. B. Cheng, W. Wen, X. Zhang, S. Wang and W. H. Huang, *Anal. Chem.*, 2018, **90**, 5075–5081.
27 X. Fu, X. Tan, R. Yuan and S. Chen, *Biosens. Bioelectron.*, 2017, **90**, 61–68.
28 H. Zhou, Y. Y. Zhang, J. Liu, J. J. Xu and H. Y. Chen, *J. Phys. Chem.*, 2012, **116**, 17773–17780.
29 L. Deng, Y. Du, J. J. Xu and H. Y. Chen, *Biosens. Bioelectron.*, 2014, **59**, 58–63.
30 Y. Yu, C. Lu and M. Zhang, *Anal. Chem.*, 2015, **87**, 8026–8032.
31 J. Liu, X. He, K. Wang, D. He, Y. Wang, Y. Mao, H. Shi and L. Wen, *Biosens. Bioelectron.*, 2015, **70**, 54–60.
32 T. Hu, X. Liu, S. Liu, Z. Wang and Z. Tang, *Anal. Chem.*, 2014, **86**, 3939–3946.
33 Y. P. Dong, Y. Zhou, J. Wang and J. J. Zhu, *Anal. Chem.*, 2016, **88**, 5469–5475.
34 M. S. Wu, L. J. He, J. J. Xu and H. Y. Chen, *Anal. Chem.*, 2014, **86**, 4559–4565.
35 H. Ma, X. Li, T. Yan, Y. Li, H. Liu, Y. Zhang, D. Wu, B. Du and Q. Wei, *ACS Appl. Mater. Interfaces*, 2016, **8**, 10121–10127.
36 J. Wang, X. Jiang and H. Han, *Biosens. Bioelectron.*, 2016, **82**, 26–31.
37 Y. P. Dong, J. Wang, Y. Peng and J. J. Zhu, *Biosens. Bioelectron.*, 2017, **89**, 1053–1058.
38 W. Zhu, M. S. Khan, W. Cao, X. Sun, H. Ma, Y. Zhang and Q. Wei, *Biosens. Bioelectron.*, 2018, **99**, 346–352.
39 J. L. Liu, M. Zhao, Y. Zhuo, Y. Q. Chai and R. Yuan, *Chem. – Eur. J.*, 2017, **23**, 1853–1859.
40 Y. P. Dong, T. T. Gao, Y. Zhou and J. J. Zhu, *Anal. Chem.*, 2014, **86**(22), 11373–11379.
41 Y. Feng, C. Dai, J. Lei, H. Ju and Y. Cheng, *Anal. Chem.*, 2015, **88**, 845–850.
42 X. Li, X. Zhang, H. Ma, D. Wu, Y. Zhang, B. Du and Q. Wei, *Biosens. Bioelectron.*, 2014, **55**, 330–336.
43 H. Dai, G. Xu, S. Zhang, L. Gong, X. Li, C. Yang, Y. Lin, J. Chen and G. Chen, *Biosens. Bioelectron.*, 2014, **61**, 575–578.
44 D. Liu, L. Wang, S. Ma, Z. Jiang, B. Yang, X. Han and S. Liu, *Nanoscale*, 2015, **7**, 3627–3633.
45 S. Y. Deng, J. P. Lei, Y. Huang, X. N. Yao, L. Ding and H. X. Ju, *Chem. Commun.*, 2012, **48**, 9159–9161.
46 W. Gu, X. Deng, X. Gu, X. Jia, B. Lou, X. Zhang, J. Li and E. Wang, *Anal. Chem.*, 2015, **87**, 1876–1881.
47 Y. H. Sha, Z. Y. Guo, B. B. Chen, S. Wang, G. P. Ge, B. Qiu and X. H. Jiang, *Biosens. Bioelectron.*, 2015, **66**, 468–473.
48 S. Zhu, X. Lin, P. Y. Ran, Q. Xia, C. C. Yang, J. Ma and Y. Z. Fu, *Biosens. Bioelectron.*, 2017, **91**, 436–440.
49 G. F. Jie, H. P. Huang, X. L. Sun and J. J. Zhu, *Biosens. Bioelectron.*, 2008, **23**, 1896–1899.
50 H. Zhou, J. Liu, J. J. Xu, S. S. Zhang and H. Y. Chen, *Chem. Soc. Rev.*, 2018, **47**, 1996–2019.
51 J. Ma, Y. H. Chen, Z. Hou, W. Jiang and L. Wang, *Biosens. Bioelectron.*, 2013, **43**, 84–87.
52 Y. J. Li, Y. Q. Li, Y. Y. Wu, F. S. Lu, Y. W. Chen and W. H. Gao, *Biosens. Bioelectron.*, 2017, **87**, 585–591.
53 L. Ge, W. X. Wang, X. M. Sun, T. Hou and F. L, *Anal. Chem.*, 2016, **88**, 2212–2219.
54 Y. Chen, Y. Xiang, R. Yuan and Y. Q. Chai, *Nanoscale*, 2015, **7**, 981–986.
55 J. Lou, S. S. Liu, W. W. Tu and Z. H. Dai, *Anal. Chem.*, 2015, **87**, 1145–1151.
56 H. Zhou, Y. Y. Zhang, J. Liu, J. J. Xu and H. Y. Chen, *Chem. Commun.*, 2013, **49**, 2246–2248.
57 L. L. Ren, H. Dong, T. T. Han, Y. Chen and S. N. Ding, *Analyst*, 2017, **142**, 3934–3941.
58 G. F. Jie, Y. Q. Qin, Q. M. Meng and J. L. Wang, *Analyst*, 2015, **140**, 79–82.
59 G. H. Zhao, X. J. Li, Y. B. Zhao, Y. Y. Li, W. Cao and Q. Wei, *Analyst*, 2017, **142**, 3272–3277.
60 S. Carrara, F. Arcudi, M. Prato and L. D. Cola, *Angew. Chem., Int. Ed.*, 2017, **56**, 4757–4761.
61 H. Cui, Y. Xu and Z. F. Zhang, *Anal. Chem.*, 2004, **76**, 4002–4010.
62 Y. C. Yu, J. J. Shi, X. C. Zhao, Z. Q. Yuan, C. Lu and J. Lu, *Analyst*, 2016, **141**, 3305–3312.
63 N. Sardesai, S. Pan and J. Rusling, *Chem. Commun.*, 2009, **33**, 4968–4970.
64 C. X. Tang, Y. Zhao, X. W. He and X. B. Yin, *Chem. Commun.*, 2010, **46**, 9022–9024.
65 B. Yang, J. P. Li, L. M. Zhang and G. B. Xu, *Analyst*, 2016, **141**, 5822–5828.
66 H. Cui, W. Wang, C. F. Duan, Y. P. Dong and J. Z. Guo, *Chem. – Eur. J.*, 2007, **13**, 6975–6984.
67 F. Li, Y. Q. Yu, H. Cui, D. Yang and Z. P. Bian, *Analyst*, 2013, **138**, 1844.

68 E. Kerr, E. H. Doeven, G. J. Barbante, C. F. Hogan, D. J. Hayne, P. S. Donnelly and P. S. Francis, *Chem. Sci.*, 2016, **7**, 5271–5279.
69 X. Zhang, H. Ke, Z. M. Wang, W. W. Guo, A. M. Zhang, C. S. Huang and N. Q. Jia, *Analyst*, 2017, **142**, 2253–2260.
70 X. Q. Lu, H. F. Wang, J. Du, B. M. Huang, D. Liu, X. H. Liu, H. X. Guo and Z. H. Xue, *Analyst*, 2012, **137**, 1416–1420.
71 P. J. Smith and C. K. Mann, *J. Org. Chem.*, 1969, **34**, 1821–1826.
72 L. J. Xiao, Y. Q. Chai, R. Yuan, H. J. Wang and L. J. Bai, *Analyst*, 2014, **139**, 1030–1036.
73 H. T. Xiong and X. W. Zheng, *Analyst*, 2014, **139**, 1732–1739.
74 Z. L. Qiu, J. Shu and D. P. Tang, *Analyst*, 2015, **140**, 5885–5890.
75 J. X. Wang, Y. Zhuo, Y. Zhou, H. J. Wang, Y. Yuan and Y. Q. Chai, *ACS Appl. Mater. Interfaces*, 2016, **8**, 12968–12975.
76 M. N. Ma, Y. Zhuo, R. Yuan and Y. Q. Chai, *Anal. Chem.*, 2015, **87**, 11389–11397.
77 M. S. Wu, H. W. Shi, J. J. Xu and H. Y. Chen, *Chem. Commun.*, 2011, **47**, 7752–7754.
78 Y. Q. Feng, F. Sun, N. N. Wang, J. P. Lei and H. X. Ju, *Anal. Chem.*, 2017, **89**, 7659–7666.
79 X. Q. Chen, W. Y. Gui, H. Liu and Q. Ma, *Analyst*, 2017, **142**, 4142–4149.
80 S. Kirschbaum-Harriman, M. Mayer, A. Duerkop, T. Hirsch and A. J. Baeumner, *Analyst*, 2017, **142**, 2469–2474.
81 Y. Chem, J. Xu, J. Su, Y. Xiang, R. Yuan and Y. Q. Chai, *Anal. Chem.*, 2012, **84**, 7750–7755.
82 Y. Y. Yang, M. A. Goetzfried, K. Hidaka, M. X. You, W. H. Tan, H. Sugiyama and M. Endo, *Nano Lett.*, 2015, **15**, 6672–6676.
83 X. Y. Jiang, H. J. Wang, H. J. Wang, Y. Zhuo, R. Yuan and Y. Q. Chai, *Anal. Chem.*, 2017, **89**, 4280–4286.
84 Y. T. Liu, J. P. Lei, Y. Huang and H. X. Ju, *Anal. Chem.*, 2014, **86**, 8735–8741.
85 G. F. Jie, K. Chen, X. C. Wang and Z. K. Lu, *RSC Adv.*, 2016, **6**, 2065–2071.
86 L. C. Peng, P. Zhang, Y. Q. Chai and R. Yuan, *Anal. Chem.*, 2017, **89**, 5036–5042.
87 P. Zhang, X. Y. Wu, R. Yuan and Y. Q. Chai, *Anal. Chem.*, 2015, **87**, 3202–3207.
88 C. Y. Xiong, W. B. Liang, Y. N. Zheng, Y. Zhuo, Y. Q. Chai and R. Yuan, *Anal. Chem.*, 2017, **89**, 3222–3227.
89 Y. Fan, X. R. Tan, X. Ou, Q. Lu, S. H. Chen and S. P. Wei, *Electrochim. Acta*, 2016, **202**, 90–99.
90 X. J. Du, D. Jiang, N. Hao, Q. Liu, J. Qian, L. M. Dai, H. P. Mao and K. Wang, *Chem. Commun.*, 2015, **51**, 11236–11239.
91 Y. Zhou, H. J. Wang, Y. Zhuo, Y. Q. Chai and R. Yuan, *Anal. Chem.*, 2017, **89**, 3732–3738.
92 M. Zhao, Y. Zhuo, Y. Q. Chai and R. Yuan, *Biomaterials*, 2015, **52**, 476–483.
93 Y. M. Lei, M. Zhao, A. Wang, Y. Q. Yu, Y. Q. Chai, R. Yuan and Y. Zhuo, *Chem. – Eur. J.*, 2016, **22**, 8207–8214.
94 X. Y. Jiang, H. J. Wang, H. J. Wang, R. Yuan and Y. Q. Chai, *Anal. Chem.*, 2016, **88**, 9243–9250.
95 Y. Cheng, Y. Huang, J. P. Lei, L. Zhang and H. X. Ju, *Anal. Chem.*, 2014, **86**, 5158–5163.
96 Z. X. Li, Y. Q. Zhou, D. P. Yan and M. Wei, *J. Mater. Chem. C*, 2017, **5**, 3473–3479.
97 Q. M. Feng, Y. Z. Shen, M. X. Li, Z. L. Zhang, W. Zhao, J. J. Xu and H. Y. Chen, *Anal. Chem.*, 2015, **88**, 937–944.
98 H. R. Zhang, J. J. Xu and H. Y. Chen, *Anal. Chem.*, 2013, **85**, 5321–5325.
99 H. R. Zhang, M. S. Wu, J. J. Xu and H. Y. Chen, *Anal. Chem.*, 2014, **86**, 3834–3840.
100 N. Hao, X. L. Li, H. R. Zhang, J. J. Xu and H. Y. Chen, *Chem. Commun.*, 2014, **50**, 14828–14830.
101 K. Shao, B. Wang, S. Y. Ye, Y. P. Zuo, L. Wu, Q. Li, Z. C. Lu, X. C. Tan and H. Y. Han, *Anal. Chem.*, 2016, **88**, 8179–8187.
102 Y. Z. Wang, N. Hao, Q. M. Feng, H. W. Shi, J. J. Xu and H. Y. Chen, *Biosens. Bioelectron.*, 2016, **77**, 76–82.
103 X. M. Fu, X. R. Tan, R. Yuan and S. H. Chen, *Biosens. Bioelectron.*, 2017, **90**, 61–68.
104 M. N. Ma, Y. Zhuo, R. Yuan and Y. Q. Chai, *Anal. Chem.*, 2015, **87**, 11389–11397.
105 Y. Q. Yu, H. Y. Zhang, Y. Q. Chai, R. Yuan and Y. Zhuo, *Biosens. Bioelectron.*, 2016, **85**, 8–15.
106 W. J. Zeng, N. Liao, Y. M. Lei, J. Zhao, Y. Q. Chai, R. Yuan and Y. Zhuo, *Biosens. Bioelectron.*, 2018, **100**, 490–496.
107 X. Yang, Y. Q. Yu, L. Z. Peng, Y. M. Lei, Y. Q. Chai, R. Yuan and Y. Zhuo, *Anal. Chem.*, 2018, **90**, 3995–4002.
108 Y. M. Lei, B. Q. Xiao, W. B. Liang, Y. Q. Chai, R. Yuan and Y. Zhuo, *Biosens. Bioelectron.*, 2018, **109**, 109–115.
109 M. H. Jiang, P. Lu, Y. M. Lei, Y. Q. Chai, R. Yuan and Y. Zhuo, *Electrochim. Acta*, 2018, **271**, 464–471.
110 Y. Zhou, M. Chen, Y. Zhuo, Y. Chai, W. Xu and R. Yuan, *Anal. Chem.*, 2017, **89**, 6787–6793.
111 J. Zhao, W. B. Liang, Y. M. Lei, Y. X. Ou, Y. Q. Chai, R. Yuan and Y. Zhuo, *Biosens. Bioelectron.*, 2017, **98**, 317–324.
112 Y. Zhou, H. Wang, Y. Zhuo, Y. Chai and R. Yuan, *Anal. Chem.*, 2017, **89**, 3732–3738.
113 F. F. Wu, Y. Zhou, H. Zhang, R. Yuan and Y. Q. Chai, *Anal. Chem.*, 2018, **90**, 2263–2270.
114 J. L. Liu, Z. L. Tang, Y. Zhuo, Y. Q. Chai and R. Yuan, *Anal. Chem.*, 2017, **89**, 9108–9115.
115 H. F. Zhao, R. P. Liang, J. W. Wang and J. D. Qiu, *Chem. Commun.*, 2015, **51**, 12669–12672.
116 Y. Huang, J. P. Lei, Y. Cheng and H. X. Ju, *Biosens. Bioelectron.*, 2016, **77**, 733–739.
117 H. M. Chen, H. Zhang, R. Yuan and S. H. Chen, *Anal. Chem.*, 2017, **89**, 2823–2829.
118 J. J. Jiang, D. Chen and X. Z. Du, *Sens. Actuators, B*, 2017, **251**, 256–263.
119 Q. W. Shang, Z. X. Zhou, Y. F. Shen, Y. Y. Zhang, Y. Li, S. Q. Liu and Y. J. Zhang, *ACS Appl. Mater. Interfaces*, 2015, **7**, 23672–23678.

120 H. J. Chen, W. Li, Q. Wang, X. Jin, Z. Nie and S. Z. Yao, *Electrochim. Acta*, 2016, **214**, 94–102.
121 L. Wu, F. Ding, W. M. Yin, J. Ma, B. R. Wang, A. X. Nie and H. Y. Han, *Anal. Chem.*, 2017, **89**, 7578–7585.
122 X. B. Feng, N. Gan, H. R. Zhang, T. H. Li, Y. T. Cao, F. T. Hu and Q. L. Jiang, *Biosens. Bioelectron.*, 2016, **75**, 308–314.
123 X. B. Feng, N. Gan, S. C. Lin, T. H. Li, Y. T. Cao, F. T. Hu, Q. L. Jiang and Y. J. Chen, *Sens. Actuators, B*, 2016, **226**, 305–311.
124 Y. Z. Wang, W. Zhao, P. P. Dai, H. J. Lu, J. J. Xu, J. Pan and H. Y. Chen, *Biosens. Bioelectron.*, 2016, **86**, 683–689.
125 Y. Chen, S. W. Zhou, L. L. Li and J. J. Zhu, *Nano Today*, 2017, **12**, 98–115.
126 Z. Y. Zhou, L. R. Xu, S. Z. Wu and B. Su, *Analyst*, 2014, **139**, 4934–4939.
127 Z. J. Lin, X. M. Chen, T. T. Jia, X. D. Wang, Z. X. Xie, M. Oyama and X. Chen, *Anal. Chem.*, 2008, **81**, 830–833.
128 J. J. Xu, P. Y. Huang, Y. Qin, D. C. Jiang and H. Y. Chen, *Anal. Chem.*, 2016, **88**, 4609–4612.
129 M. S. Wu, Z. Liu, H. W. Shi, H. Y. Chen and J. J. Xu, *Anal. Chem.*, 2014, **87**, 530–537.
130 K. F. Chow, F. Mavré, J. A. Crooks, B. Y. Chang and R. M. Crooks, *J. Am. Chem. Soc.*, 2009, **131**, 8364–8365.
131 L. R. Xu, Y. Li, Y. Y. He and B. Su, *Analyst*, 2013, **138**, 2357–2362.
132 Y. Li, L. R. Xu, Y. Y. He and B. Su, *Electrochem. Commun.*, 2013, **33**, 92–95.
133 J. Zhang, P. P. Chen, X. Y. Wu, J. H. Chen, L. J. Xu, G. N. Chen and F. F. Fu, *Biosens. Bioelectron.*, 2011, **26**, 2645–2650.
134 E. G. Hvastkovs, M. So, S. Krishnan, B. Bajrami, M. Tarun, I. Jansson, J. B. Schenkman and J. F. Rusling, *Anal. Chem.*, 2007, **79**, 1897–1906.
135 S. Krishnan, E. G. Hvastkovs, B. Bajrami, D. Choudhary, J. B. Schenkman and J. F. Rusling, *Anal. Chem.*, 2008, **80**, 5279–5285.
136 H. R. Zhang, Y. Z. Wang, W. Zhao, J. J. Xu and H. Y. Chen, *Anal. Chem.*, 2016, **88**, 2884–2890.
137 R. Liu, C. S. Zhang and M. Liu, *Sens. Actuators, B*, 2015, **216**, 255–262.
138 M. Liu, D. Wang, C. L. Liu, R. Liu, H. J. Li and C. S. Zhang, *Sens. Actuators, B*, 2017, **246**, 327–335.
139 K. Song, P. Huang, C. L. Yi, B. Ning, S. Hu, L. M. Nie, X. Y. Chen and Z. H. Nie, *ACS Nano*, 2015, **9**, 12344–12348.
140 J. Wang, T. Wei, X. Y. Li, B. H. Zhang, J. X. Wang, C. Huang and Q. Yuan, *Angew. Chem., Int. Ed.*, 2014, **126**, 1642–1646.
141 L. R. Xu, Z. Y. Zhou, C. Z. Zhang, Y. Y. He and B. Su, *Chem. Commun.*, 2014, **50**, 9097–9100.
142 L. R. Xu, Y. Li, S. Z. Wu, X. H. Liu and B. Su, *Angew. Chem., Int. Ed.*, 2012, **124**, 8192–8196.
143 J. Tan, L. R. Xu, T. Li, B. Su and J. M. Wu, *Angew. Chem., Int. Ed.*, 2014, **53**, 9822–9826.
144 F. Deiss, C. N. LaFratta, M. Symer, T. M. Blicharz, N. Sojic and D. R. Walt, *J. Am. Chem. Soc.*, 2009, **131**, 6088–6089.
145 N. P. Sardesai, J. C. Barron and J. F. Rusling, *Anal. Chem.*, 2011, **83**, 6698–6703.
146 M. Sentic, M. Milutinovic, F. Kanoufi, D. Manojlovic, S. Arbault and N. Sojic, *Chem. Sci.*, 2014, **5**, 2568–2572.
147 S. M. Pan, L. L. Zhao, J. B. Schenkman and J. F. Rusling, *Anal. Chem.*, 2011, **83**, 2754–2760.
148 D. P. Wasalathanthri, D. D. Li, D. H. Song, Z. F. Zheng, D. Choudhary, I. Jansson and J. F. Rusling, *Chem. Sci.*, 2015, **6**, 2457–2468.
149 J. Wang, G. Liu and A. Merkoçi, *J. Am. Chem. Soc.*, 2003, **125**, 3214–3215.
150 J. R. Miao, Z. J. Cao, Y. Zhou, C. Lau and J. Z. Lu, *Anal. Chem.*, 2008, **8**, 1606–1613.
151 H. Li, Z. J. Cao, Y. H. Zhang, C. W. Lau and J. Z. Lu, *Analyst*, 2011, **136**, 1399–1405.
152 Z. Y. Guo, T. T. Hao, S. P. Du, B. B. Chen, Z. B. Wang, X. Li and S. Wang, *Biosens. Bioelectron.*, 2013, **44**, 101–107.
153 F. F. Han, H. Jiang, D. J. Fang and D. C. Jiang, *Anal. Chem.*, 2014, **86**, 6896–6902.
154 B. Zhou, Y. Y. Qiu, Q. Q. Wen, M. Y. Zhu and P. H. Yang, *ACS Appl. Mater. Interfaces*, 2017, **9**, 2074–2082.
155 P. Zhang, Z. F. Lin, Y. Zhuo, R. Yuan and Y. Q. Chai, *Anal. Chem.*, 2017, **89**, 1338–1345.
156 L. C. Peng, P. Zhang, Y. Q. Chai and R. Yuan, *Anal. Chem.*, 2017, **89**, 5036–5042.
157 Y. M. Nie, P. Zhang, H. J. Wang, Y. Zhuo, Y. Q. Chai and R. Yuan, *Anal. Chem.*, 2017, **89**, 12821–12827.
158 W. B. Liang, C. C. Fan, Y. Zhuo, Y. N. Zheng, C. Y. Xiong, Y. Q. Chai and R. Yuan, *Anal. Chem.*, 2016, **88**, 4940–4948.
159 W. B. Liang, M. Z. Yang, Y. Zhuo, Y. N. Zheng, C. Y. Xiong, Y. Q. Chai and R. Yuan, *Chem. Sci.*, 2016, **7**, 7094–7100.
160 D. M. Cate, J. A. Adkins, J. Mettakoonpitak and C. S. Henry, *Anal. Chem.*, 2015, **87**, 19–41.
161 A. W. Martinez, S. T. Phillips, M. J. Butte and G. M. Whitesides, *Angew. Chem., Int. Ed.*, 2007, **46**, 1318–1320.
162 G. Lei, J. H. Yu, S. G. Ge and M. Yan, *Anal. Bioanal. Chem.*, 2014, **406**, 5613–5630.
163 W. Y. Gao, M. Saqib, L. M. Qi, W. Zhang and G. B. Xu, *Curr. Opin. Electrochem.*, 2017, **3**, 4–10.
164 Y. Zhang, L. Li, L. N. Zhang, S. G. Ge, M. Yan and J. H. Yu, *Nano Energy*, 2017, **31**, 174–182.
165 X. W. Zhang, J. Li, C. Q. Chen, B. H. Lou, L. L. Zhang and E. K. Wang, *Chem. Commun.*, 2013, **49**, 3866–3868.

